

Authors' response to the first referee

- 1) Referee Comment: 1. In the manuscript a cosine fit is applied to wind lidar data acquired during VAD scans in order to estimate the mean wind speed and direction. Such a data analysis method requires the assumption of horizontal homogeneity of the wind vector, as also stated by the authors. However, I am wondering to which extent this homogeneity is expected over the urban landscape of Paris. I think that a discussion on the terrain heterogeneity is missing from the article. In this direction, I think that it would be constructive to add an elevation map of the area over which the scanning wind lidar was acquiring measurements. This would provide an insight to which extent the observed spatial variations of the wind are related to temporal fluctuations of the wind and/or due to changes of the terrain elevation.
- 1) Authors' Response: 1. The lidar scans were covering the urban area of Paris as it can be seen in Figure 1b of the manuscript. In Paris there is a height limit for the buildings. Please see Figure 1 of the supplementary materials with the height limits of the buildings in Paris from the official Planning Department of the city of Paris, 2006. The Jussieu site is highlighted by the green text symbol. The buildings in the centre of Paris range between 25 and 37 m and rarely reach or exceed 50 m. So despite being an urban area, it is rather homogeneous. We have added the elevation map of the area in P5 as Figure 2 in the manuscript. In Figure supplementary materials you can also find the map with the altitude of the beam, see Figure 2 of the supplementary materials.
- 2) RC: In this context and regarding the data analysis: a. A statistical parameter is required to specify the representativeness of the fit used in the VAD scan. In the manuscript it is stated that the RMSE values of the estimated fit have been calculated but they are not stated in the document. b. Did the authors perform a quality check of the acquired data? Do they apply any SNR filtering to the acquired radial wind speed prior the application of the data analysis?
- 2) AR: a. The RMSE and similar statistical parameters for the fit quality evaluation incorporate in their values the difference between the radial wind speed and the fitted function which is the parameter we are interested in. Therefore, it is complicated to use such a parameter to characterize the quality of the fit. What we did instead, it was to select the bad cases based on the symmetry of the radial wind field. An example of a bad case is showcased in Figure 4a of the manuscript, when the radial wind field is not symmetric and as a result the radial wind speed shows a more chaotic behaviour when plotted against the azimuth angle (Figure 4, manuscript). On the contrary the good cases were selected for symmetric radial wind fields as the one presented in Figure 3 of the manuscript.
- b. We forgot to include this information. We considered only the radial wind speed values for which the carrier-to-noise ratio (CNR) is higher than -27 dB. The values where $CNR < -27$ dB were filtered out since the radial wind speed had anomalously high values, 2 times or higher compared to the rest of the radial wind observations. In P5 L149-151, the following sentence has been added "For this study, the radial wind speed values for which the carrier-to-noise ratio is lower than -27dB ($CNR < -27$ dB) were disregarded since they were anomalously high, exceeding the values of the rest of the radial wind field by two times or more."
- 3) RC: 2. The subtraction of the mean wind speed from the radial wind speeds does not compensate the fact that the individual measurements along the scanning pattern are the result of the projection of the instantaneous wind vector to the line-of-sight of the wind lidar. Therefore, the term turbulent wind field could lead to a misinterpretation. The authors should clearly state that they measure the high frequency fluctuations of the radial wind speed.
- 3) AR: It is true that using the word turbulent can be misleading since we do not observe very small scales. We will make clear in the manuscript that what we observe are medium-to-large fluctuations and coherent structures (mlf-cs). However, we will state that these are associated to a turbulent atmosphere.
- 4) RC: Specific Comments: P2 Line 28. The reference of Roth 2007 is a review of the atmospheric turbulence studies over urban landscapes and it doesn't directly discuss how the pollution concentration in urban environment is dependent on the weather and on the turbulence. A reformulation of this sentence is suggested for a clarification.
- 4) AR: The first paragraph will be removed along with the references. We will instead emphasize the effect of the turbulent structures in the pollutants' dispersion. In P1 L31-46, the following text has been added: "Several studies have been carried out to examine the effect of the coherent turbulent structures in the dispersion of pollutants by utilizing boundary layer simulations. The results of these studies indicate that the coherent structures can play a significant role in the pollutants' concentrations (Aouizerats et al., 2011; Soldati, 2005). Furthermore, (Sandeepan et al., (2013) have demonstrated via

simulations that the pollutants' concentrations can alternate from low to high during coherent structures events. It is therefore important to be able to identify structures in the atmosphere and observe them in an efficient and consistent way.”.

55 5) RC: P3 Line74. Why is it relevant if the campaigns are short-term or long-term? And what is the time scale of these two types of campaigns that it is relevant for the topic of this study?

5) AR: We used an example of a short term study to show that so far lidars have been used to observe coherent structures for short periods since the analysis of a large dataset is very time-consuming. On the other hand, the example of a long-term study is mentioned to show that it provides us only point measurements instead of the whole wind field over an area. Thus we wanted to highlight the benefits of our study. In order to clarify the limitations of the long-term study, we have included the following sentence in P3 L82-83 “However, their study is limited to point measurements instead of a larger wind field that it is possible to observe via a lidar.”

65 6) RC: P3 Line95. I am not sure that the two references of Kumer 2014 and Veselovskii et al. 2016 are the appropriate to be used here. In none of them there is an analytical explanation of the wind lidar instrument as it is stated. I suggest replacing them with more relevant references. An example could be the work of: Cariou, J. P., R. Parmentier, M. Valla, L. Sauvage, I. Antoniou, and M. Courtney. "An innovative and autonomous 1.5 μm Coherent lidar for PBL wind profiling." In *Proceedings of 14th Coherent Laser Radar Conference*. 2007.

6) AR: Cariou et al, 2007 has replaced the references of Kumar and Veselovskii in P4 L109 as it is more appropriate.

70

7) RC: P3 Line 101. It is stated that “The duration of each scan was 3 minutes which is sufficiently short for the observation of structures”. Could the authors elaborate more on this statement?

7) AR: In P4 line 115, the word “fast” will replace the initial “short”. Furthermore, the sentence “The duration of each scan was 3 minutes which is sufficiently short for the observation of structures” has been rephrased to “The duration of each scan was 3 minutes which is sufficiently fast for the observation of coherent structures, as their lifespan is several minutes.”

75

8) RC: P4 Line 102. The authors state that the maximum range of the scans reached 5 km. However, in none of the figures that they have included in the manuscript the range ever reaches 5 km. The most common range in their data is between 2 – 2.5 km. Can the authors explain why is this happening?

80 8) AR: We have used the $\text{CNR} < -27\text{dB}$ filtering. Please see also the reply 2b.

9) RC: P4 Line111. Table 2. A list of scanning patterns is included here that are not used in this study. In addition, the purpose of each scanning pattern is included without explaining the reasoning for their selection. I would suggest to either remove this table. If the authors wish to keep it then I suggest that they should elaborate more in the text about it.

85 9) AR: We acknowledge that the presentation of the entire scanning sequence can be confusing for the reader, therefore the Table 2 in P5 has been modified to include only the information for the PPI and the DBS scans. We have also removed the 90° elevation angle from the table as it was not part of the DBS scanning method. The latter scanning method is also important for this study as the DBS scans revealed the high wind shear cases during night. The sentence in P4 L111 “Table 2 showcases the implemented scanning methods during the VEGILOT campaign” has replaced the initial “Table 2 showcases the scanning sequence as it was implemented during the VEGILOT campaign.”. Additionally, a brief description of the DBS scan will be added to the text. In particular, the following sentence has been added in P4 line 122-125: “It was also important for this study to retrieve observations regarding the vertical wind shear. For this purpose, the Doppler beam swinging (DBS) scanning method was implemented. This method was consisted of four line of sight beams at azimuth angles of 0°, 90°, 180° and 270° with an elevation angle of 75° and it was applied twice. The duration of the four direction beams emission was approximately 15 seconds.”.

95

10) RC: P4 Line120. The “offset” refers to the vertical wind speed component? What does it mean that a is much smaller than b ? Is this a common observation over the whole scanning plan? And what kind of a values does the application of the model result in?

100 10) AR: The offset is indeed associated to the vertical wind speed. The radial wind speed analysed in its' wind components for a line of sight beam with azimuth angle θ and elevation angle ϕ will be:

$$Vr = u \cos\theta \sin\phi + v \sin\theta \sin\phi + w \cos\phi, \text{ where } u \text{ is the longitudinal, } v \text{ is the transverse}$$

and w is the vertical wind component respectively. The offset is associated to the parameter $w \cos\phi$ (Thubois et al. 2018, [Study of the configurations and scanning strategies of Doppler Lidars for providing wind and aerosol/cloud profiles](#)). Since the elevation angle of the PPI scans was 1° and not 0° we included this parameter in the fit function. However, it is much smaller than the b component which is associated to the horizontal wind. So the horizontal wind is still dominant. This is a common observation over the whole scanning plan. The value of the offset is around 10 times smaller than the amplitude and ranges according to the value of the amplitude from 0.05 to 0.5 m/s.

110 11) RC: P6. Line156-157. It is not clear how the unaligned thermals are dependent on the increased solar radiation measurements.

AR: The increased solar radiation measurements result in surface heating which we typically observe during fair weather cumuli conditions. The phrase in P7 L195 has been modified to "Regarding unaligned thermals, solar radiation measurements, signifying fair cumuli weather conditions."

115

12) RC: P6. Line 163. How do the authors estimate the value of the wind shear? Also, shouldn't the units of the wind shear be seconds to the power of -1?

120 12) AR: The DBS observations provided us the zonal u and meridional v winds. The horizontal wind was computed from these components from the formula: $V_{\text{hor}} = \sqrt{u^2 + v^2}$. The formula has been included in the text as Equation 3 in P7. The wind shear was estimated from the vertical profile of V_{hor} by subtracting the local minima from the local maxima above it, near the surface. The units have been corrected to s^{-1} .

125 13) RC: P6. Line 166. The authors in P5. Line 133 state that the VAD method could not be applied in the data acquired during the night, especially at those occasions where the mean wind speed was less than 2 m/s. Does this mean that only cases with mean wind speed higher than 2 m/s were selected?

130 13) AR: The VAD method can be applied regardless of the mean wind speed values as long as the radial wind speed field is symmetric. It is true however that when the mean wind speed is lower than 2 m/s then the radial wind field has the risk to not be symmetric. For the training ensemble, regarding streaks, rolls and thermals only cases with moderate winds were selected (5-8 m/s) whereas for the category others cases with weak winds below 2 m/s were included. We are currently preparing a separate study with the physics of the structures based on the whole classification from this methodology. The results show that we observe winds below 2 m/s mostly during the others category. More particularly the results are: 7 out of the 1145 streaks cases, 0 out of 420 rolls cases, 67 out of the 900 thermals cases and 670 out of the 2112 others cases.

135 14) RC: P6. Line 167. How well was the mean direction and speed estimated through the VAD method in the selected cases? I suggest adding a statistical parameter that describes the representativeness of the applied fit (equation 1) to the measured data (e.g. RMSE).

140 14) AR: As we previously stated statistical parameters as the RMSE are not appropriate for the evaluation of the fit since the interesting parameter for us is the difference between the observation and the fit. We instead selected the training ensemble based on how well symmetric or not was the radial wind field and by plotting random rings for each scan to confirm good fits as displayed in Figure 3 or a bad fit as in Figure 4 of the manuscript.

15) RC: P7. Line 170. It is difficult to understand the scale of the Modis colour images. Would it be possible to either add a scale or mark on the images the scanning area?

15) AR: In P8 in Figures 5d and 5e, the scanning area has been marked on the MODIS images.

145

16) RC: P7. Line 176. I recommend describing very shortly the texture analysis especially in the context of remote sensing. It would be useful to add any references in the introduction regarding the previous applications of this type of analysis to remote sensing data.

150 16) AR: In P3 L86-88, we have added the following brief description: “Texture analysis is an effective way to evaluate the distribution of the values within an image (Castellano et al., 2004). It is widely used in various scientific fields in order to classify images, covering meteorology (Alparone et al., 1990), medical studies (Holli et al., 2010) and forestry (Kayitakire et al., 2006).”.

17) RC: P8. Line 181-182. What is the logic behind the selection of this particular values for defining the contrast?

155 17) AR: We wanted to enhance the contrast of the structures. For this reason, we had to select the bins in such a way that the difference between positive and negative values will be more apparent. We have tried more configurations. The selection of only 2 bins (one positive, one negative), led to a less successful classification of the different types of structures as the 2 bins give a 2 by 2 co-occurrence matrix. The size of the co-occurrence matrix is important in this case, since from the Equations 2, 3 and 4 of the manuscript, it is evident that the texture analysis parameters also depend on the distance between the bins i, j .
160 The classification error in this case was around 18%. The selection of the 4 bins (one bin including all the negative values below -0.5 m/s, one bin between -0.5 m/s and 0, one bin between 0 and $+0.5$ m/s and one bin including all the positive values above $+0.5$ m/s) did not really improve the results with the error remaining around 18%. The selection of 8 bins reduced the error significantly. The selection of one bin including all the negative values below -0.5 m/s, six bins equally distributed between -0.5 m/s and $+0.5$ m/s and one bin including all the positive values above $+0.5$ m/s allows us to enhance the difference
165 between the positive and negative values while keeping the distance between the bins i, j . We did not try to select more than 8 bins because we believe that it will not be useful to increase the number of bins near 0. It is in our future plans however to automatize this part as well. We would like to include an algorithm in our method in order to find the optimal selection of bins that minimizes the classification error.

170 18) RC: P10. Line 243. The authors state that 60 cases of “other” patterns are used during the supervised machine learning step. They argue that this is necessary because “it is expected to be the dominant category in the classification”. I am not sure that I understand what it is meant with this statement. I suggest having this part a bit more explained. Furthermore, how is the mean wind speed and direction estimated in these cases? As it is stated the VAD was not successfully applied to this data.

175 18) AR: When we were analysing the results, we observed that the chaotic type of patterns (see Figure 3 of the supplementary materials) was the most common type. The algorithm can be sensitive to an unbalanced training ensemble. It is preferable to select a training ensemble based on the expected results (Kubat, 2017 p.194). Therefore, even for the bad cases, the VAD method was selected for the estimation of the mean wind speed and wind direction. In Figure 4 of the supplementary materials, a fitted function for a non-symmetric field is displayed. We can still obtain the mean wind direction from this figure, but the patterns will have the chaotic look as in Figure 3 of the supplementary materials.

180

19) RC: P10. Line 225. How do the authors explain the change in the slope of the homogeneity curve that is observed for absolute azimuth angles larger than 45 degrees?

185 19) AR: The angle represents also the distance between two grid points. For 45° angles or above, the distance between two grid points are n rows away whereas below 45° they are $n-1$, $n-2$ etc. We have prepared an illustration of an ideal case, Figure 5 of the supplementary materials. We hope that it is clear. Keep in mind that the Figure 7 of the manuscript refers to the third neighbour which is equivalent to 150 m distance between the grid points.

20) RC: P10. Line 240. Could the authors add a reference to the literature describing the “supervised machine learning methodology”?

190 20) AR: In P11 L281, the following references have been added:

“Bonamente, M. Statistics and analysis of scientific data, Springer, 2017, 318 p., DOI:10.1007/978-1-4939-6572-4;

Gareth James, Daniela Witten, Trevor Hastie, Robert Tibshirani, An Introduction to Statistical Learning with Applications in R, Springer Texts in Statistics, 2013, 426 p, DOI: 10.1007/978-1-4614-7138-7

Kubat M. An Introduction to Machine Learning, Springer, 2017, <https://doi.org/10.1007/978-3-319-63913-0>”

21) RC: P11. Line 265. *How do the authors physically explain this result? A low RMSE in the cosine fit, couldn't also mean that the mean wind speed and direction are not estimated correctly?*

21) AR: This result show that according to the algorithm, the different shapes of the patterns in the radial turbulent wind field are more significant for the classification of the structures than the physical parameters. The wind values range from 1 m/s to 14 m/s. Therefore, a higher RMSE does not necessarily mean a worse fit, but it may be caused due to this scale difference.

200

22) RC: P12. Line 291. *It is stated that "there were scarcely any rolls cases observed at night". However, in the sentence 288 it is written that for the classification of this study the authors "consider only thermals and rolls during daytime". To my understanding there is an inconsistency between the two statements. Can this be explained better?*

22) AR: For the training ensemble only thermals and rolls during daytime were selected. However, the classification of all the data was made based on the five texture analysis parameters displayed in Figure 8 of the manuscript. As time is not included in the classifiers, the algorithm can classify the patterns at any time of the day but still few cases of rolls and thermals were classified during the night. This result is an indication that the classification is working as intended. In a study of the physical properties of the structures, rolls and thermals during night will be excluded.

210

23) RC: P13. Line 312. *In the conclusions the author state that time, wind speed and the cosine fit RMSE of the VAD method were not selected by the algorithm for the classification. However, in the results presented in figure 9 there is a time dependency in the detection of certain patterns (e.g. thermals and rolls). Could the authors comment why the inclusion of the time as a classification parameter would not improve further their results?*

23) AR: The algorithm finds the best combination of parameters that minimize the classification error and time was not one of the five parameters as it can be seen in Figure 8 of the manuscript. By including the time as a parameter the classification error will not be reduced.

215

24) RC: P13. Line 318. *Given the fact that one PPI scan lasts for 3 minutes and occurs every 18 means, can the authors explain how does the acquired data set contribute to the comprehension of the development of coherent structures?*

220

24) AR: The lifespan of streaks can be several tens of minutes and for rolls it can be hours. Even with this time gap between the observations we believe that it is still interesting to study the transitions between the different types of structures. For example, we have vertical lidar observations between the PPI scans and we can study the development of the atmospheric boundary layer height with regards to the type of the structures.

225

25) RC: Technical Corrections: *General: There is a small inconsistency on the way that figures are referred to. Sometimes they are used parenthesis after the number of the Figure to denote a subfigure and sometimes are not.*

25) AR: All the subfigures have been corrected in order to keep consistent naming. The number of the subfigure is now followed by the corresponding letter e.g. "Figure 1a".

230

26) RC: P2 Line 34. *I think that the statement "Futhermore, . . ." is a self-evident. I would suggest removing it. Also, I would suggest to add the reference of (Hussain, 1983) at the end of the previous sentence.*

26) AR: In P2 line 34, the sentence: "Furthermore time-averaged statistics calculations." has been removed. The reference of (Hussain, 1983) now refers to the sentence in P2 L28-29: "The principal aspect that determines a coherent structure is the maintenance of the phase-averaged vorticity of the turbulent fluid mass over the spatial extend of the flow structure."

235

27) RC: P2 Line 37. *"and the lower"*

27) AR: In P2 line 42 "and the lower" has replaced "and lower".

- 240 28) RC: P3 Line 72. I suggest reformulating this sentence. It is not clear to the reader how is the two-dimensional autocorrelation function was used. Also, I suggest changing the sentence “the observation of the scans by eye” to “visual observation of the scans”.
- 28) AR: In P3 L75-77, the sentence “They combined quantitative characteristics of the coherence such as the integral scales and the anisotropy coefficients, obtained by a two-dimensional autocorrelation algorithm, with the visual observation of the scans.” has replaced the initial “They combined a two-dimensional autocorrelation function with the observation of the scans by eye”.
- 245
- 29) RC: P3 Line76. Change “month” to “months”
- 29) AR: In P3 line 81 “months” has replaced “month”.
- 250
- 30) RC: P3 Line83. The “Section 0” should change to “Section 3”
- 30) AR: In P3 line 96 “Section 3” has replaced “Section 0”.
- 31) RC: P3 Line86. The word “two” is used as a noun modifier and therefore the word month should be in singular form.
- 255 31) AR: In P3 L100, the phrase “A two-month measurement campaign” has replaced the initial “A two-months campaign”.
- 32) RC: P3 Line96. I suggest to change the text “The lidar is sensitive only to the” to “A wind lidar is measuring the”
- 32) AR: In P4 line 110, the phrase “A wind lidar is measuring the” has replaced the initial “The lidar is sensitive only to the”.
- 260 33) RC: P3 Line100. Change the “for a” to “with a”.
- 33) AR: In P4 L113 “with a” has replaced the initial “for a”.
- 34) RC: P4 Line103. I think that it is more grammatically correct to either use the past tense or the passive form of the “rise” verb.
- 265 34) AR: In P4 L121 “the beam rise” has been rephrased to “the beam was risen”.
- 35) RC: P5 Line132. The authors state that due to the surface heterogeneity the VAD method can be applied in some cases. A surface heterogeneity will introduce an error in the VAD method regardless the wind speed.
- 270 35) AR: We have probably phrased this in a wrong way. As it can be seen in Figure 2 of the supplementary materials, there are some hills in the limits of the scanning range but with low elevation. We have not study what could be the orographic effect in the wind speed as this would require model simulations. In P6 L168-170, the following sentence had been added: “Troude et al. (2002) and Lemonsu and Masson (2002) have performed numerical weather simulations in the area of Paris and have observed that during low wind conditions (below 3 m/s) the orographic effect and the urban heat island effect could be the main drivers for the local wind speed.”.
- 275
- 36) RC: P5 Line132. I suggest that the “Jussie site” is changed to “The Jussie site”.
- 36) AR: In P6 L167 “The Jussieu site” has replaced “Jussie site”.
- 37) RC: P5 Line138. Figure 3 caption. Change the “a case” to “A case”, also a add a tab space between (a) and “Radial”.
- 280 37) AR: In P6 L174 “A case” has replaced “a case” and a tab space has been inserted between (a) and “Radial” in the caption of Figure 4.

38) RC: P6. Line149. “Sec” should be replaced by “Section”.

38) AR: In P7 line 149 “Section” has replaced “Sec”.

285

39) RC: P6. Line 164. I suggest to re-write the sentence “For many cases, the wind shear was accompanied by turbulent streaks pattern” and specify for which particular wind shear values were streaks detected.

40) RC: P6. Line165. The part of the sentence “so or the training ensemble” should be rewritten.

39-40) AR: In P7 L204, the sentence “For the training ensemble, only night cases when streaks patterns (Figure 5c) were accompanied by wind shear higher than 2 s^{-1} were selected.” has replaced the initial “For many cases, the wind shear was accompanied by turbulent streaks patterns (Figure 4c) so or the training ensemble, only night cases of streaks were selected to ensure that wind shear was the primary factor for the generation of turbulence.”.

290

41) RC: P10. Line 230. “fore” should be changed to “for”.

295 41) AR: In P11 L271 the word “for” has replaced the initial “fore”.

42) RC: P11. Line251 – 253. The authors state the higher number of dimensions relative to the number of patterns lead to the “curse of the dimensionality problem”. I suggest to re-write it by using appropriate scientific statements.

42) AR: The "curse of the dimensionality problem" is a scientific term, which is common in statistics/data science domain. We think that it is relevant here.

300

43) RC: P11. Line 259. Correct the “Section 0”.

43) AR: “Section 0” has been removed from that part of the text.

305 44) RC: P12. Table 5 caption: I suggest changing the “eye-made” to “visual”.

44) AR: In P13 the word “visual” has replaced the initial “eye-made” in the caption of Table 5.

45) RC: P12. Line 290. The coherent structures don’t have a preference. They are formed under favourable atmospheric conditions. I suggest commenting the result of Figure 9 on that basis.

310 45) AR: This was undoubtedly a bad way to phrase it. In P14 L352-356, we made the following changes in the text: “It is evident that despite time was not one of the selected classifiers, the number of occurrences of the structures show a distribution that can be associated to the atmospheric conditions. More particularly, rolls and thermals were mainly classified during day. This result is noteworthy as these structures are linked to a well-developed atmospheric boundary layer during day. On the contrary, there were scarcely any rolls cases observed at night and a few unaligned thermals were classified at night.” on the
315 initial “It is evident that despite time was a much less significant classifier compared to the curves parameters, the structures show a time preference. There were scarcely any rolls cases observed at night, though a few unaligned thermals were classified at night.”

315

46) RC: P15. Line 386. “Lemone” should be changed to “LeMone”. Also, necessary information of the article (e.g. journal) is missing.

320

46) AR: In P118 L488, the name has been corrected and the missing information has been added. The complete reference now is: “LeMone, M., 1972. The structure and dynamics of the horizontal roll vortices in the planetary boundary layer. J. Atmos. Sci. 30, 1077–1091. [https://doi.org/10.1175/1520-0469\(1973\)030<1077:tsadoh>2.0.co;2](https://doi.org/10.1175/1520-0469(1973)030<1077:tsadoh>2.0.co;2)”

325 Authors' response to the second referee

330 47) RC: *As I understand from the first paragraph in the introduction, comprehension of the flow physics it is important for monitoring atmospheric pollution. However, the physics identified here, in the form of coherent structures, are not related with bad pollution conditions, since the latter might fall in the "Other" category, and their physics are not clear from the study.*

47) Author Response: We recognize that the first paragraph can be misleading and therefore it has been removed. We focus only on the effect of turbulent structures in the pollutants' dispersion. See also the response (4) to the first author.

335 48) RC: *The motivation of the study should be stressed from the beginning. Only when we arrive to the conclusions we can read some of the potential application of this approach. (line 316 of the text).*

340 48) AR: We want to show that it is possible to identify and classify these structures based solely on the patterns from the fluctuations of the radial wind speed data by combining texture analysis and supervised machine learning. For this reason, we have added the following text in the Introduction P3 L83-93 last paragraph: "This study aims to identify the medium-to-large fluctuations and coherent structures (mlf-cs) on single Doppler lidar horizontal scans and develop an automatic classification process based on the combination of texture analysis and a supervised machine learning technique, namely the Quadratic Discriminate Analysis (QDA), in order to handle large datasets. Texture analysis is an effective way to evaluate the distribution of the values within an image (Castellano et al., 2004). It is widely used in various scientific fields in order to classify images, covering meteorology (Alparone et al., 1990), medical studies (Holli et al., 2010) and forestry (Kayitakire et al., 2006). There is a lack of long-term studies of structures based on lidar observations and the aforementioned automatic classification process can stimulate the interest in this research field. More particularly, it could facilitate the statistical analysis of the physical parameters of the structures, e. g. the structure size as a function of the planetary boundary layer (PBL) height. Furthermore, it will enable us to study the transitions between structures and how these are associated to the atmospheric conditions. Finally, the impact of the structures on pollutants' concentrations could be examined for long-term studies under stable and unstable conditions."

350

49) RC: *In general, the term turbulence and turbulence fields are used frequently in the text, but the range gate resolution of the lidar scanner is 50m at a height of 75m above ground level. Turbulence and its most energetic eddies might fall within this length scale. Almost all turbulence fluctuations are filtered out by the lidar due to spatial averaging. What we can clearly see from lidar observations is medium-to-large scale fluctuations and coherent structures rather than turbulence.*

355 49) AR: We have replaced the term turbulence to the suggested medium-to-large fluctuations and coherent structures (mlf-cs) as we do not observe small scale turbulence and the reader can be confused. Nonetheless, we have stated that these structures are associated to a turbulent atmosphere.

50) RC: *I miss a paragraph describing how data quality was assured.*

360 50) AR: Unfortunately, during the VEGILOT campaign there was no other wind data measurements for comparison. The closest weather station with available data for the same period, as our study, is located in Montsouris, 20 km away from the centre of Paris.

51) RC: *Did you use a CNR/SNR threshold for filtering?*

365 51) AR: We used the CNR filtering. The radial wind speed values below -27 dB were anomalously high and therefore excluded from the computations. See also response (2b) to the first author.

52) RC: *What was the data recovery rate during the two months of measurements?*

370 52) AR: The lidar was taking measurements continuously for the two-month period for the scanning sequence presented in Table 2 of the manuscript. There was no pausing of the measurements during this period.

53) RC: It is not clear from the text how the radial wind speed fluctuations are calculated. What does “stronger radial wind speed” mean? A larger absolute value? It seems to me that the sign might come from the combination of u and $\cos(\theta)$. One suggestion is to put this definition as equations.

375 53) AR: The radial wind field has values with a positive sign when the wind moves away from the lidar and negative sign when it moves toward the lidar. In order to be consistent throughout the field when we study the fluctuations, we have to make a sign convention that guarantees for example that the radial wind speed with a value of 6 m/s and the radial wind speed with a value of -6 m/s will be part of the same pattern. Therefore, we compared the absolute values and we derive the sign convention of Figure 2b. We have add the following formula in the manuscript as Equation 2 P5 L162: $u'_r = |u_r(\theta)| - |f(\theta)|$, where f is
380 the fitted function for the corresponding azimuth angle θ .

54) RC: Since the wind direction is obtained from equation (1) it would be possible to work with the streamwise component u instead of the radial wind speed u_r . It is not clear from the results, what is the relative importance of non-distinguishable structures, bad fittings, and bad data (low CNR/SNR signals) in the “Others” category. The authors give some information
385 about what it seems to be the reason of one group of cases to belong to this category (bad fitting of cosine function), but no threshold on this fitting error is given.

54) AR: We did not perform an extensive analysis of the data for the “Others” category. This category was selected exclusively to separate the not interesting patterns. The bad cases were not selected based on the quality of the fit but rather in the symmetry of the whole radial wind field. For the category “others” in the training ensemble, we selected 53 bad cases with an
390 asymmetrical radial wind field and 7 cases of a symmetrical field where the structures were non-distinguishable. In Figure 3a of the manuscript, it is apparent that the wind field is not symmetrical and that the VAD method would not be applied efficiently. Nevertheless, it can still be applied as you can see in Figure 4 of the supplementary materials (it is the same with Figure 4b of the paper along with a cosine fitted function). Since we are interested in the fluctuations (difference between the observation and the fitted curve) it is very difficult to characterize the quality of the fit by using a parameter such as the RMSE
395 that contains these fluctuations. We are currently working on a study for the physical parameters of the structures based on the classification of this study. We found that for 670 out of the 2112 others cases the mean wind speed is lower than 2 m/s. On the other hand, for the streaks it is only 7 out of the 1145 cases, for rolls 0 out of 420 cases and for thermals 67 out of the 900 cases. This is very interesting as the mean wind speed was not one of the classifiers.

400 55) RC: I miss more elaboration in the description of the texture parameters used for classification, namely, why they might be relevant and if they were relevant in the end. The feature selection process is also not very clear. Cross validation is well known and well explained, but the text explaining the outcome as well as the figure used in that regard are confusing. A brief description of the machine learning technique used could be useful for clarity.

55) AR: The description of the texture parameters has been added in the manuscript, in particular in P10 L251-255:
405 “Correlation indicates the existence of linear structures in the image, with high values associated to a large amount of linear structure in the image. Contrast reveals the local variations in an image, where a large amount of variations leads to high values. Homogeneity is self-explanatory and the high values represent a homogeneous image. Finally, energy measures the uniformity of an image with the highest values corresponding to constant or periodic forms (Haralick et al., 1973; Yang et al., 2012).”.

410 These texture parameters are frequently used in patterns based image classification. As we mention in our manuscript we selected these four parameters inspired by the study of Srivastava et al. (2018). They used the same parameters to distinguish stripes among others patterns. By plotting the texture parameters against the azimuth angle φ (angle of the comparing neighbour points), we observed a prominent peak for the elongated patters for $\varphi =$ mean wind direction. The relevant parameters are showcased in Figure 8 of the manuscript.

415 Regarding the feature selection process by the algorithm the following text has been added in P10-11 L287-293: “The greedy algorithm of stepwise forward selection was used in the article, which is the standard and frequently used method of reduction of the feature space. As indicated in (Sokolov et al., 2020), it can be formulated as follows. The features are divided into two groups - accepted in the classification model and remaining, for which an estimate of the possibility of acceptance into the model is checked. Features from the set of “remains” are consecutively added to the model and corresponding estimations of
420 the classification error are calculated. From the received set of errors, the minimum is chosen and compared with the error of the previous model. If a significant reduction of the error occurred, then the corresponding feature is accepted into the model, if not then the process stops.”

For the specific machine learning technique, we utilized, we have included a brief description in P11 L283-286: “Quadratic discriminant analysis or normal Bayesian classification (Hastie et al., 2009) is the parametric approach implying that

425 probability density functions (PDF) belong to the family of normal distributions. It is a classical algorithm of the supervised machine learning, based on the principle of maximum likelihood. The general idea is to estimate the PDF for each class, and then select the most probable class (Kubat, 2017).”

430 56) RC: *Conclusions section. In my opinion, this section should be read in a positive rather than negative way. Example: it should focus on the relevant parameters discovered (which need a bit more explanation in the corresponding section) rather than the ones excluded by the study. The sections describing the methodology used-which need some improvement-are already clear, and no repetition is needed. Same with the results highlighted.*

435 56) AR: It is very important for us to stress the positives of this study and therefore we have modified the conclusions to comment on the relevant parameters. In P15 L376-384, the following text has been added: ” More particularly, these parameters were the amplitude of the 2nd-neighbour homogeneity curve and the amplitude of the 4th-neighbour contrast curve which were associated to the prominent peaks of the elongated patterns (streaks, rolls). Furthermore, the integral of the 18th-neighbour contrast curve and the integral of the 8th-neighbour correlation curve which could distinguish, for example, chaotic patterns (“others”) with high contrast and lower values of correlation between neighbour points compared to an enclosed homogeneous (thermals). Finally, the symmetry of the 2nd-neighbour homogeneity curve revealed the importance to align the mlf-cs fields to the mean wind direction. Another striking outcome of the QDA classification was the variety of the classifiers in terms of distance between the grid points. The 2nd-neighbour translates in a distance between two grid points equivalent to 100 m and for the 18th-neighbour to 900 m. This is essential for the classification between patterns with different sizes such as streaks and rolls.”

445 57) RC: *2 Specific comments Page 1 Line 12. Change “manually” to “visually”.*

57) AR: In P1 L12 the word “visually” has replaced the initial “manually”.

58) RC: *Page 1 Line 15. Change “and installed” to “installed”.*

450 58) AR: In P1 L15 the word “and” has been removed with the phrase now reading “by a scanning Doppler lidar (LEOSPHERE WLS100) installed”.

59) *Page 1 Line 16. It would be better to reword this sentence, maybe “The turbulent component of radial wind speed is estimated using. . .over 4577 scans.*

455 59) In P1 L16-17 the sentence “The lidar recorded 4577 quasi-horizontal scans for which the turbulent component of the radial wind speed was determined using the velocity azimuth display method.” has been rephrased to “The mlf-cs of the radial wind speed are estimated using the velocity azimuth display method over 4577 quasi-horizontal scans.”.

460 60) RC: *Page 1 Line 18-21. I am not sure what the sentence describing the training set adds to the abstract if not combined with the next one. It is better to state directly the unsupervised algorithm used instead of using parenthesis. It might be better to rephrase this in a more concise way.*

465 60) AR: In P1 L19-23 the text: “The differences between the three types of structures Using the 10-fold cross validation method, the classification error was estimated to be about 9.2% for the training ensemble and 3.3% in particular for streaks. ” has been rephrased to “The differences between the three types of structures The algorithm was able to classify successfully about 91% of the cases based solely on the texture analysis parameters. The algorithm performed best for the streaks structures with a classification error equivalent to 3.3%.”.

61) RC: *Page 1 Line 23. What are the remaining 20*

61) AR: The remaining 20% are the unaligned thermals. We wanted to highlight the results only for the rolls and streaks as we find in literature that the majority of the studies focus on these two types of coherent structures.

470

62) RC: *Page 2 Line 26. Change “step for” to “step towards”.*

62) AR: We have removed the first paragraph of the introduction and instead address only the impact of turbulent structures on pollutants' dispersion.

475 63) RC: Page 2 Line 32. A coherent structure is defined according to its phase-averaged rather than its instantaneous vorticity. I also suggest moving the Hussain 1983 reference to this sentence. A coherent structure needs to maintain its phase-averaged vorticity rather than its time-averaged vorticity or form.

480 63) AR: In P2 line 32 the adverb “instantaneously” was referring to the phase-averaged vorticity. In order to avoid confusion, the text in P2 L28-29: “The principal aspect that determines a coherent structure is the instantaneously space and phase correlated vorticity of the turbulent fluid mass over the spatial extend of the flow structure. Furthermore, a coherent structure must maintain its form for a time period sufficient for time-averaged statistics calculations (Hussain, 1983).” has been rephrased to “The principal aspect that determines a coherent structure is the maintenance of the phase-averaged vorticity of the turbulent fluid mass over the spatial extend of the flow structure (Hussain, 1983).”.

485 64) RC: Page 2 Line 35. Please specify that this is the case of atmospheric flow. Other structures are observed at laboratory scale (also in the atmosphere but not so relevant for momentum or scalar fluxes), like hairpins, or hairpin trains. Include a reference to Hutchins and Marusic (2006) and Adrian (2007).

490 64) AR: We have included the following text in P2 L36-39: “The term coherent structures in the aforementioned studies refers exclusively in the atmospheric flow and it is the main focus in this study. This term is also encountered in studies at laboratory scale described as hairpins or packets (Adrian, 2007; Hutchins and Marusic, 2007), but these are out of the scope of this study.”.

65) RC: Page 2 lines 37-44. Consider reordering the sentences here for a more fluent reading. Maybe starting the paragraph from sentence in line 41?

495 65) AR: We have rearranged the sentences in P2 L40-44. The first sentence of the paragraph is now: “Turbulent streaks are structures aligned with the horizontal wind with alternating stripes of stronger horizontal wind associated with a subsidence and stripes of weaker horizontal wind associated with an ascendance (Khanna and Brasseur, 1998).”.

500 66) RC: Page 2 line 45. How is it that you identify rolls in the mixed layer, with sizes from few to dozen kilometers, with scans at surface layer height (75m) with spatial coverage of less than 2 kilometers?. Is this description coherent with what you are identifying?

66) AR: In the introduction we give general information about the rolls and we think it is important to address their scale. In P7 L192-193, we have added the following sentence: “It is important to note that we observed the occurring patterns near the surface, hence near the lower part of the rolls.”

505 67) RC: Page 2 lines 57-65. Since you are using lidar instead of radars it would be better to shorten the scanning pattern description using some of the given references, since they have to do only with the history on scanning patterns. There are more recent references of this regarding lidars. Cariou (2007) and Vasiljevic (2016).

510 67) AR: We have included few more lidar studies references. More particularly, in P2-3 L68-70 the following text has been added “It has been well established that the PPI method can also be applied to Doppler lidars (Cariou et al., 2007; Vasiljević et al., 2016) with the possibility to compute the mean wind profile by using a modified version of the VAD method as it has been demonstrated in the studies of Banta et al., (2002) and Chai et al., (2004).”.

68) RC: Page 3 line 72. Replace “by eye” by “visual inspection” or similar.

68) AR: In P3 L77 the phrase “visual observation of the scans” has replaced the initial “by eye”.

515 69) RC: Page 3 line 73. More than time-consuming, it might be non-systematic.

69) AR: In P3 L77-78 the sentence has been modified to: “However, the subjective classification by observing the images is a time-consuming approach and non-systematic.”.

520 70) RC: Page 3 line 74. You meant “A less time-consuming” approach? What height was the met mast?

70) AR: The term less expensive refers to the sonic anemometers themselves without including the met mast. The data for the Barthlott et al (2007) study was taken at a 30 m tower.

525 71) RC: Page 3 line 78. “This study aims to identify turbulent coherent structures from single Doppler lidar horizontal scans”. Also, please introduce here what is texture analysis (roughly maybe) and what machine learning technique you are using.

71) AR: Regarding the texture analysis, we have added a brief description. See also response (16) to the first referee. For the machine learning technique, we also added a brief description. See also response (55) to the second referee.

72) RC: Page 3 line 83. Section 0 must read section 3, here and in the rest of the text.

530 72) AR: In P3 L96 Section 3 has replaced the initial Section 0 and it has been corrected throughout the text.

535 73) RC: Page 3 line 86-91. It should read “measurement campaign”. Move “in Paris” to the end of the sentence, modified to “in the urban area of Paris”. Remove the url of leosphere to the reference section maybe. More than only sensitive to the radial component, the lidar does measure and it is intended to measure only the radial component. Lidars technology and its operation principle is well known, use references (Cariou, maybe write ts paragraph in amore concise way, being specific in the corresponding table than in the text here, which is a bit confusing.

73) AR: AR: In P3 L100, the phrase “A two-month measurement campaign” has replaced the initial “A two-months campaign”. In P3 L102 the phrase “in the urban area of Paris” has been inserted. The Cariou (2007) reference has replaced the initial “Kumer et al. (2014) and Veselovskii et al. (2016)” in P4 L109.

540

74) RC: Page 3 line 101. I would say fast instead of short. Also, what type of structures and why this time window?

74) AR: We refer to coherent structures, in P4 L115 the sentence “The duration of each scan was 3 minutes which is sufficiently fast for the observation of coherent structures with a lifespan of several minutes.” Has replaced the initial “The duration of each scan was 3 minutes which is sufficiently short for the observation of structures.”.

545 The time-window of 3 min is the result of the selection of the 2° azimuth angle resolution. We wanted to combine a high spatial resolution with a time-window that would allow us to observe coherent structures.

75) RC: Page 4 line 121. What is the reason behind a is small for your case?.

550 75) AR: The parameter a is associated to the vertical wind speed, more particularly with the parameter $w\cos\phi$ of the radial wind speed analysed in its' wind components for a line of sight beam with azimuth angle θ and elevation angle ϕ :

$Vr = u \cos\theta \sin\phi + v \sin\theta \sin\phi + w\cos\phi$, where u is the longitudinal, v is the transverse

and w is the vertical wind component respectively. The offset is associated to the parameter $w\cos\phi$ (Thubois et al. 2018, [Study of the configurations and scanning strategies of Doppler Lidars for providing wind and aerosol/cloud profiles](#)).

In our case the elevation angle is only 1° thus a is around 10 times smaller than the parameter b throughout our data.

555

76) RC: Page 5 Figure 2. Why the reach of the lidar is 2 km and no 5 km?.

76) AR: Due to the CNR<-27dB filtering. See also response (2b) to the first referee.

560 77) RC: Page 5 line 134. Is it possible to specify the fraction of cases with low winds, and its relative importance to the number of bad fittings?. I miss an analysis of stability conditions, since it seems that stable conditions affect the most.

77) AR: As we mentioned previously, we examine the symmetry of the radial wind field rather than the individual bad fit for each ring. We are currently working on a separate study for the physical properties of the structures and the atmospheric conditions under their occurrences. We are interested in this result as well, however we have not finished the study yet. Nonetheless, the preliminary results show that low winds (<2 m/s) are the main cause for non-symmetric radial wind fields.

565

78) RC: Page 6 line 143. Actually, for rolls, it is the opposite. Ascending motions bring low momentum to higher levels, reducing the speed, and vice versa.

570 78) AR: This has been corrected in P3 L40-41: “Turbulent streaks are structures aligned with the horizontal wind with alternating stripes of stronger horizontal wind associated with a subsidence and stripes of weaker horizontal wind associated with an ascendance (Khanna and Brasseur, 1998).”.

79) RC: Page 6 line 146. Since rolls and streaks both present areas of alternating low/high momentum with elongated shape, their main difference is their extent. What is the criteria to differentiate between them? The clouds formation shape from MODIS was used, as I understand, only for a fraction of the cases included in the training dataset.

575 79) AR: For the training ensemble we combined the patterns of the fluctuations of the radial wind speed field with physical characteristics that indicate the existence of a structure. For streaks we selected cases with wind shear higher than 2 s^{-1} near the surface and for rolls, cases when clouds streets were formed over Paris as observed from MODIS satellite images. Due to the scarcity of satellite data, in order to select 30 cases of rolls we also included the consecutive cases of the cloud streets ones, as long as the patterns persisted.

580

80) RC: Page 6 line 161-165. Wind shear is defined as du/dz with $1/s$ units, could you clarify what definition you are using here? Additionally, streaks are present in turbulent flow as well, beyond stable conditions, why do you focus in cases with low turbulence energy (stable conditions)? It seems that high shear due to jets is only one among several mechanisms.

585 80) AR: The units have been corrected to s^{-1} . For the computation of the horizontal wind, we used the DBS observations. In particular the horizontal wind was computed by the formula: $V_{hor} = \sqrt{u^2 + v^2}$, where u is the zonal and v is the meridional winds. We included this formula on the manuscript in P7 L203 as Equation 3. The wind shear was estimated from the vertical profile of V_{hor} .

We only used night streaks because the wind shear is a clear indication for the existence of streaks. As the algorithm only uses the five texture analysis parameters for the classification (Figure 8 of the manuscript), it shouldn't affect the results.

590

81) RC: Page 6 line 166. How many cases did you use for the “Other” category? From table 5 seems that they are around 60, the double. What is the reason for such big number?. Can this influence the final classification output? This is explained in section 4, but it should be clear from here.

595 81) AR: We used 60 cases which is double compared to the rest. The reason is that some of the machine learning algorithms are sensitive to the balance of classes in the training data (see Kubat 2017, p 194). If one category is dominant but for the training ensemble all categories are represented by the same number of cases, then the algorithm can overestimate or underestimate a category. Nevertheless, we also tried a training ensemble with all the categories represented by 30 cases and the results were similar.

600 82) RC: Page 7 Figure 4. What is the scale of map in (d) and (e)?

82) AR: We have added the scanning area in Figures 5d and 5e of the manuscript.

83) RC: Page 7 line 176. Could you introduce what texture analysis is first? Additionally, since “Others” had a poor fitting and then uncertain wind direction, how did you align them with 0 degrees?

605 83) AR: We have included a brief description of texture analysis as showcased in response (16) to the first referee.

The VAD method was used even for the bad cases, as the radial wind field in this case fell in the category of not interesting. As it can be seen in Figure 4 of the supplementary materials, it is still possible to fit a cosine function even for a bad fit and but the patterns are not interesting as illustrated in Figure 3 of the supplementary material.

610 84) RC: Page 7 line 180. Eight bins were chosen for increased contrast. Why eight?, could you develop more on this?. What is the effect of the number of bins in the output?

84) AR: The scope was to enhance the contrast of the structures for a better visualization of the alternating positive and negative areas in the radial turbulent wind field as we explained analytically in response (17) to the first referee.

615 85) RC: Page 8 line 185. The procedure for the construction of the CM matrix is a bit confusing. Could you write it in a more concise way?

85) AR: In P9 L226-227 the following sentence “The rows and columns of the CM represent the wind levels from 1 to 8, whereas the cells contain the frequency of the combination of two neighbour pixels in the image” has replaced the initial “The rows and columns of the CM represent the wind levels from 1 to 8, whereas the cells contain the number of occurrences of neighbour pairs with values corresponding to the row and column index.”.

620

86) RC: Page 9 line 212. Is it possible to elaborate more on the 4 parameters described?. It is not clear only from the equations what their characteristics are.

625

86) AR: The following text has been added in the manuscript in P10 L251-255: “Correlation indicates the existence of linear structures in the image, with high values associated to a large amount of linear structure in the image. Contrast reveals the local variations in an image, where a large amount of variations leads to high values. Homogeneity is self-explanatory and the high values represent a homogeneous image. Finally, energy measures the uniformity of an image with the highest values corresponding to constant or periodic forms (Haralick et al., 1973; Yang et al., 2012).”.

630

87) RC: Page 10 Figure 6. The notation of the azimuth angle is different from the text. Why does homogeneity grow after 45 degrees for all categories? The definition of homogeneity says that CMs with large values in the diagonal might result in larger values of this parameter. The diagonal from table 3 to 4 decrease because of azimuth angle. Should homogeneity decrease monotonically from 0 to +/- 90 degrees?. Can you elaborate more on this?. How many cases are represented for each category in the figure? Only one scan? An average from many cases?

635

87) AR: The notation of the azimuth angle in the y axis of the Figure 7 in P11 has been corrected. The angle also represents the distance between two grid point. For 45° angles or above, the distance between two grid points are n rows whereas below 45° they are n-1, n-2 etc. We have included an ideal case in Figure 5 of the supplementary material. Regarding whether the homogeneity should decrease monotonically from 0 to +/- 90 degrees, that depends on the case and on the order of the neighbour. When we have elongated patterns then yes we can see the prominent peak at 0° as we see in Figure 7 for the streaks and in some degree for rolls but not so much for thermals and others. In the ideal case of Figure 5 in the supplementary material it is also possible to see how the values of the co-occurrence matrix change according to the periodicity of the patterns.

640

88) RC: Page 10 line 231. Notation is a bit weird here.

645

88) AR: The maximum and minimum refer to the azimuth angle φ . We have modify Equation 8 in P11 of the manuscript as follows:

$$\text{Hom. Amp}(n) = \max_{\varphi}(\text{Hom}(\varphi, n)) - \min_{\varphi}(\text{Hom}(\varphi, n))$$

89) RC: Page 10 line 241. The description of the training set might be better place in section 3. Why is it expected that “other” category should double the rest? Please elaborate more on this.

650

89) AR: The preliminary analysis of patterns showed that “others” class is approximately twice abounded than each other class. We decided to double the number of examples “others” class in the training dataset, as some of machine learning algorithms are sensitive to the balance of classes in the training data (see Kubat 2017, p 194).

655 90) RC: Page 11 Figure 7. This figure is very confusing and not self-explanatory at all. Please give more information in its caption, relative to the number in parenthesis (neighbor order I suppose), state that they are all or a few of the final parameters used.

660 90) AR: In P 13 Figure 8 the following caption has been added: “Parameters selected to minimize the classification error of the training ensemble by the QDA method. From left to right: Amplitude of the homogeneity for the 2nd-neighbour, integral of the contrast for the 18th-neighbour, amplitude of the contrast for the 4th-neighbour, integral of the correlation of the 8th-neighbour and symmetry of the homogeneity for the 2ndneighbour.” has replace the initial “Figure 7: Texture analysis parameters selected to minimize the classification error of the training ensemble by the QDA method.”.

91) RC: Page 12 Table 5. Change “eye-made” to a better term, like visual classification or similar.

91) AR: In P13 the word “visual” has replaced the initial “eye-made” in the caption of Table 5.

665 92) RC: Page 12 line 286. It is not clear if streaks were also detected during daytime, since the previous definition of the training set (line 162) says only night-time, but figure 9 says the opposite. Same for rolls and thermals. In summary, the constraint you talk about (day-time rolls and thermals, night-time streaks) does concern only the training set definition?

670 92) AR: Up until Figure 8 of the manuscript we showed the results for the training ensemble, where we only considered rolls and thermals during day and streaks during the night. So the classification error of the algorithm in Figure 8 refers to the training ensemble. The algorithm was able to classify our training ensemble successfully for approximately 91% for the texture analysis parameters of Figure 8. Then we use these parameters to classify all the 4577 scans and the results are presented in Figures 9 and 10 of the manuscript, thus we detect streaks during the day and thermals and rolls during the night.

675 93) RC: Page 12 line 292. If I am correct, you tried to explain thermals during night, not others during days. Only the last word in the sentence, “reverse”, explains this. Moreover, can you elaborate more on what is the reason behind the erroneous classification of thermal as “others”? During stable conditions turbulent eddies are smaller, structures also show smaller length-scales. However, mean wind can show slight differences with no directional preference, and they can look like thermals (see Shah and Bou-Zeid, 2014).

680 93) AR: The category “others” includes the patterns that cannot be classified to one of the three turbulent structures type. It is possible to have a not symmetrical wind field, thus a bad case, during the day as well. In fact, 10 bad cases of the training ensemble for the category “others” occurred during the day. The physics behind the misclassification are very interesting. However, in our case the misclassification is linked to the shape of the patterns. It is possible that another texture analysis parameter could improve the distinction between these two types.

685 94) RC: Page 13 line 295. Stable cases during night show buoyant forces opposing vertical momentum flux and turbulence generation. Mechanical turbulence does die out under stable conditions. Mechanical turbulence destruction by buoyancy is the dominant mechanism, not the opposite.

690 94) AR: In P14 L360-362 we have added the following sentence “This was also expected as the nocturnal low level jets is a main driving factor for the formation of streaks and we observed the occurrence of wind shear higher than 2 s^{-1} over Paris for 20 out of the 62 nights during the VEGILOT campaign.”.

95) RC: Page 13 line 314. So thermals are not turbulent?. Why do you separate rolls and steaks form thermals? Does it has to do with pollution transport or something similar?

695 95) AR: Rolls and streaks are the focus on many boundary layer studies. In the specific sentence, we wanted to emphasize the regularity of observing coherent structures over Paris during the period of our study. Moreover, in the study we are currently working on with regards to the physics of the structures, the transition between the structures for particular cases (e.g. low level jets, cloud streets etc.) will be one of the focal points.

List with all the changes

700

In P1 L8 the affiliation “Institute of Numerical Mathematics, Russian Academy of Sciences, Moscow Russia” has changed to “Marchuk Institute of Numerical Mathematics Russian Academy of Sciences, Moscow, Russia”.

705

In P1 L12-L21, P3 L96-L110, P4 L127-L142, P5 L165, P6 L176, P7 L188-L189-L190-L193-196, P8 L225, P9 L231, P9 L238, P9 L241, P12 L297-L314, P14 L373-L374, P15 L391, P16 L417-L420 the term “Turbulent structures” has changed to “Medium-to-large fluctuations and coherent structures (mlf-cs)”.

In P1 L13 the word “manually” has changed to “visually”.

In P1 L14-L20-L28, P2 L70, P3 L85-L86-L92-L94, P14 L374, P16 L414-L418 the word “turbulent” has been removed.

In P1 L16 the word “and” has been removed.

710

In P1 L17-18 the sentence “The lidar recorded using the velocity azimuth display method” has been replaced by the sentence “The mlf-cs of the radial wind speed over 4577 quasi-horizontal scans”.

In P1 L24 the phrase “namely the” has been added before “quadratic discriminate analysis” which is now without a parenthesis.

In P1 L24-25 the sentence “Using the 10 fold cross validation in particular for streaks” has been replaced by the text “The algorithm was able classification error equivalent to 3.3%”.

In P2 L32-35 the paragraph “The understanding of the connection low turbulence (Kallos et al, 1993).” has been removed.

715

In P2 L37 the phrase “instantaneously space and phase correlated” has changed to “maintenance of the phase-averaged”.

In P2 L39-40 the sentence “Furthermore, a coherent averaged statistics calculations (Hussain, 1983)” has been removed.

In P2 L42-49 the text “Several studies have been out of the scope of this study.” has been added.

In P2 L50-51 the sentence “Turbulent streaks are structures with an ascendance (Khanna and Brasseur, 1998).” was moved to the beginning of the paragraph.

720

In P2 L59 the reference “Lemone, 1972” changed to “LeMone, 1972”.

In P3 L79-81 the sentence “The PPI method ... Doppler lidars.” changed to “It has been well in the studies of Banta et al., (2002) and Chai et al., (2004).”

In P3 L87-89 the sentence “They combined a two dimensional of the scans by eye.” changed to “They combined quantitative characteristics visual observation of the scans.”

725

In P3 L90 the phrase “and non-systematic” has been added following the phrase “time-consuming approach”.

In P3 L94-95 the sentence “However, their study observe via a lidar” has been added.

In P3 L97-98 the phrase “based on the combination Quadratic Discriminate Analysis (QDA)” has been added.

In P3 L99-107 the text “Texture analysis is an effective and unstable conditions.” has been added.

In P3 L107 the word “It” changed to “The classification method”.

730

In P3 L108 the expression “2-month” changed to “two-month”.

In P3 L110 “Section 0” changed to “Section 3”.

In P4 L114 the expression “A two-months campaign” changed to “A two-month measurement campaign” & “in Paris” has been removed.

In P4 L116 the phrase “in the urban area of Paris” has been added.

735

In P4 L124 the references “Kumer et al. (2014) and Veselovskii et al. (2016)” changed to “Cariou et al., 2007”.

In P4 L124 the phrase “The lidar is sensitive only to” changed to “A wind lidar is measuring”.

In P4 L126 the phrase “scanning sequence as it was implemented” changed to “implemented scanning methods”.

- In P4 L129 the word “for” changed to “with”.
- 740 In P4 L130 the word “short” changed to “fast” & the phrase “observation of structures” changed to “observation of coherent structures with a lifespan of several minutes”.
- In P4 L132-136 the text “It is noteworthy that homogeneous urban surface” has been added.
- In P4 L136 the verb “rise” changed to “was risen”.
- In P4 L137-141 the text “It was also important approximately 15 seconds” has been added.
- 745 In P5 L150-153 Table 2 changed to showcase only the scanning methods PPI and DBS that was used for this study & the caption “Scanning sequence during VEGILOT” changed to “Scanning methods selected during VEGILOT”. Additionally, the elevation of “90°” has been removed from the DBS properties as it was not selected for the experiment.
- In P5 L153 the “Figure 2” has been added to showcase the ground altitude map for the scanning area. As a result, the numbering of the Figures has been modified accordingly throughout the manuscript.
- In P5 L166-169 the text “A parameter that indicates 3 km.” has been added.
- 750 In P6 L172 the “Equation 2” has been added along with the text “and it was computed f is the fitted curve.”. As a result, the numbering of the Equations has been modified accordingly throughout the manuscript.
- In P6 Figure 3d & in P8 Figures 5a, 5b, 5c & in Figures 6a, 6b the title of the colorbar “turbulent radial wind field” changed to “Mlf-cs field”.
- In P6 L178 the word “The” has been added in the beginning of the paragraph.
- 755 In P6 L179 the expression “homogeneity of the wind field” changed to “regional wind flow”.
- In P6 L179-181 the sentence “Troude et al for the local wind speed” has been added.
- In P7 L192 the words “ascending” and “descending” have been switched.
- In P7 L199 “Sec. 4.1” changed to “Section 4.1”.
- In P7 L206-207 the sentence “It is important to note lower part of the rolls” has been added.
- 760 In P7 L209 the phrase “signifying fair weather conditions” has been added.
- In P7 L214 the units “m/s” changed to “s⁻¹”.
- In P7 L215-217 the formula for the horizontal wind speed computed from the DBS observations has been added as Equation 3 accompanied by the sentence “The horizontal wind speed via the expression.”. As a result, the numbering of the Equations has been modified accordingly throughout the manuscript.
- 765 In P8 L217-219 the sentence “For many cases generation of turbulence” changed to “Consequently, the wind shear were selected.”.
- In P8 L223-224 the sentence “Regarding rolls VAD method was applicable.” has been added.
- In P8 L227 the expression “turbulence pattern type” changed to “structure type”.
- 770 In P9 L243 the phrase “number of occurrences of neighbour pairs with values corresponding to the row and column index” changed to “frequency of the combination of two neighbour pixels in the image”.
- In P10 L268-271 the text “Correlation indicates the existence of linear structures in the image, with high values associated to a large amount of linear structure in the image. Contrast reveals the local variations in an image, where a large amount of variations leads to high values. Homogeneity is self-explanatory and the high values represent a homogeneous image. Finally, energy measures the uniformity of an image with the highest values corresponding to constant or periodic forms (Haralick et al., 1973; Yang et al., 2012).” has been added.
- 775 In P11 Equation 8 the notation “ φ ” has been added.
- In P12 L298 the expression “The Quadratic Discriminant Analysis” changed to “The QDA”.
- In P12 L300-311 the text “QDA or normal Bayesian then the process stops.” has been added.
- In P12 L315-316 the text “The algorithm can be was preferred (Kubat, 2017).” has been added.

- 780 In P12-13 L328-341 the text “In particular, these parameters for chaotic ones (“others”)” changed to “Analytically, these parameters horizontal sizes differ.”.
- In P13 L347-348 the sentence “The significant parameters with different sizes” changed to “Furthermore it demonstrates with different sizes.”.
- In P13 L351-354 the caption of Figure 8 “Texture analysis parameters by the QDA method” changed to “Parameters selected for the 2nd neighbour.”.
- 785 In P13 L356 the sentence “The algorithm allowed classifying correctly about 91% of the training ensemble.” has been added.
- In P14 L364 the “eye made” changed to “visual”.
- In P14-15 the text “It is evident that despite time was a much less significant classified at night.” changed to “It is evident that despite time was not one of the selected classified at night.”.
- 790 In P15 L386-387 the sentence “This was also expected formation of streaks” changed to “This was also expected during the VEGILOT campaign.”.
- In P15 L391-393 the sentence “The current study single Doppler lidar” changed to “The current study supervised machine learning technique”.
- In P15 L393-394 the sentence “More particularly a two months 1° elevation” has been removed.
- 795 In P15 L394-399 the text “The VAD method was used ... enclosed patterns (unaligned thermals)” changed to “By applying the VAD method enclosed patterns (unaligned thermals)”.
- In P15 L400-401 the sentence “In order to apply and unaligned thermals” changed to “A training ensemble And unaligned thermals.”.
- In P15 L402 “For this purpose” changed to “Subsequently”.
- 800 In P15 L403 the phrase “to the training ensemble in” has been added & “and” has been removed.
- In P15 L404 the sentence “The algorithm allowed analysis parameters as predictors.” changed to “The results showed analysis parameters as predictors.”.
- In P15-16 L405-414 the text “More particularly, these parameters such as streaks and rolls” has been added.
- In P16 L428-L430 the initials HD have been added to the authors’ contribution.
- 805 In P16 L445-446 the acknowledgement “Experiments presented in this paper supported by SCoSI/ULCO (Service COmmun du Système d’Information de l’Université du Littoral Côte d’Opale).” has been added.
- In P16 L447 the acknowledgement “This study was funded by RFBR, project number 20-07-00370.” has been added.
- In P17 L449-457 the references of “Adrian, 2007, Alparone et al., 1990, Aouizerats et al., 2011, Banta et al., 2002” have been added.
- 810 In P17 L460-461 the reference of “Bonament,e 2017” has been added.
- In P17 L466-472 the references of “Cariou et al., 2007, Castellano et al., 2004, Chai et al., 2004” have been added.
- In P17 L488-490 the reference of “Holli et al., 2010” has been added.
- In P18 L500 the reference of “Kallos et al., 1993” has been removed.
- In P18 L500-504 the references of “James et al., 2000, Kayitakire et al., 2006” have been added.
- 815 In P18 L513 the reference of “Kumer et al., 2014” has been removed.
- In P18 L513 the reference of “Kubat, 2017” has been added.
- In P18 L518 the “LeMone” reference has been corrected.
- In P18 L520 the reference of “Lemonsu and Masson, 2002” has been added.
- In P18 L531 the reference of “Roth, 2007” has been removed.
- 820 In P18-19 the references of “Saint-Pierre et al., 2010, Sandeepan et al., 2013” have been added.

In P19 L538 the reference of “Soldati, 2005” has been added.

In P19 L545 the reference of “Troude et al., 2002” has been added.

In P19 L549 the reference of “Veselovskii et al., 2016” has been removed.

In P19 L549 the reference of “Vasiljević et al., 2016” has been added.

825

830

Detecting turbulent structures on single Doppler lidar large datasets: an automated classification method for horizontal scans

Ioannis Cheliotis¹, Elsa Dieudonné¹, Hervé Delbarre¹, Anton Sokolov¹, Egor Dmitriev², Patrick Augustin¹, Marc Fourmentin¹

¹ Laboratoire de Physico-Chimie de l'Atmosphère (LPCA), UR 4493, Université du Littoral Côte d'Opale (ULCO), Dunkirk, France

²~~Institute of Numerical Mathematics, Russian Academy of Sciences~~ Marchuk Institute of Numerical Mathematics Russian Academy of Sciences, Moscow, Russia

10 Correspondence to: Ioannis Cheliotis (ioannis.cheliotis@univ-littoral.fr)

Abstract

~~Turbulent-Medium-to-large fluctuations and coherent~~ structures (mlf-cs) can be observed using horizontal scans from single Doppler lidar or radar systems. Despite the ability to detect the structures manually-visually on the images, this method would be time-consuming on large datasets, thus limiting the possibilities to perform studies of the ~~turbulent~~-structures properties over more than a few days. In order to overcome this problem, an automated classification method was developed, based on the observations recorded by a scanning Doppler lidar (LEOSPHERE WLS100) ~~and~~-installed atop a 75-m tower in Paris city centre (France) during a 2-months campaign (September-October 2014). ~~The lidar recorded 4577 quasi-horizontal scans for which the turbulent component of the radial wind speed was determined using the velocity azimuth display method. The mlf-cs of the radial wind speed are estimated using the velocity azimuth display method over 4577 quasi-horizontal scans.~~

15 Three ~~turbulent~~-structures types were identified by visual examination of the wind fields: unaligned thermals, rolls and streaks. A learning ensemble of 150 ~~turbulent-mlf-cs~~ patterns was classified manually relying on *in-situ* and satellite data. The differences between the three types of structures were highlighted by enhancing the contrast of the images and computing four texture parameters (correlation, contrast, homogeneity and energy) that were provided to the supervised machine learning algorithm, namely the -(quadratic discriminate analysis). ~~Using the 10 fold cross validation method, the classification error was estimated to be about 9.2% for the training ensemble and 3.3% in particular for streaks. The algorithm was able to classify successfully about 91% of the cases based solely on the texture analysis parameters. The algorithm performed best for the streaks structures with a classification error equivalent to 3.3%.~~

20 The trained algorithm applied to the whole scan ensemble detected ~~turbulent~~-structures on 54 % of the scans, among which 34 % were coherent ~~turbulent~~-structures (rolls, streaks).

30 1. Introduction

The understanding of the connection between atmospheric physics and air pollutants' dispersion is a necessary step for improving regulation and monitoring of atmospheric pollution. The level of pollution is highly dependent on the weather and particularly on turbulence (Roth, 2007). The pollution peaks occur during weather conditions where the pollutants' dispersion is restrained e.g. stagnant conditions, low altitude thermal inversion, low turbulence (Kallos et al., 1993).

35 Turbulent flows are motions characterized by high unpredictability. Nevertheless, coherent structures are developed in these flows (Tur and Levich, 1992). The principal aspect that determines a coherent structure is the ~~instantaneously space and phase correlated maintenance of the phase-averaged~~ vorticity of the turbulent fluid mass over the spatial extend of the flow structure (Hussain, 1983). ~~Furthermore, a coherent structure must maintain its form for a time period sufficient for time-averaged statistics calculations (Hussain, 1983).~~ The most typical types of coherent structures are presented in the review of
40 Young et al (2002), who classified structures into three characteristic types: turbulent streaks, convective rolls and gravity waves. ~~Several studies have been carried out to examine the effect of the coherent turbulent structures in the dispersion of pollutants by utilizing boundary layer simulations. The results of these studies indicate that the coherent structures can play a significant role in the pollutants' concentrations (Aouizerats et al., 2011; Soldati, 2005). Furthermore, (Sandeepan et al., (2013) have demonstrated via simulations that the pollutants' concentrations can alternate from low to high during coherent structures events. It is therefore important to be able to identify structures in the atmosphere and observe them in an efficient and consistent way. The term coherent structures in the aforementioned studies refers exclusively in the atmospheric flow and it is the main focus in this study. This term is also encountered in studies at laboratory scale described as hairpins or packets (Adrian, 2007; Hutchins and Marusic, 2007), but these are out of the scope of this study.~~

~~Turbulent streaks are structures aligned with the horizontal wind with alternating stripes of stronger horizontal wind associated with a subsidence and stripes of weaker horizontal wind associated with an ascendance (Khanna and Brasseur, 1998).~~ The high wind shear between the surface layer and ~~the~~ lower planetary boundary layer (PBL) can lead to the formation of the turbulent streaks in the surface layer that may extend to the mixed layer. Neutral or near-neutral stratification favours the formation of streaks though they may also form during stable and unstable conditions (Khanna and Brasseur, 1998). The physics behind their formation differs as the contribution of buoyancy varies in relation to the atmospheric conditions (Moeng
55 and Sullivan, 1994). Formation, evolution and decay of streaks are rather short, equivalent to several tens of minutes, before they regenerate. The average streak spacing is usually hundreds of meters (Drobinski and Foster, 2003).

In the mixed layer, horizontal roll vortices, also known as convective rolls, develop roughly aligned with the mean wind (LeMone, 1972)~~(Lemone, 1972)~~. Favourable conditions for the development and maintenance of convective rolls are the spatial variations of surface-layer heat flux, the low-level wind shear and the relatively homogeneous surface characteristics
60 (Weckwerth and Parsons, 2006). As the rolls rotate in the vertical plane, they generate ascending and descending motions. These motions under convective conditions can form clouds in rows separated by clear sky areas known as cloud streets which is a characteristic visual feature used to identify rolls (Lohou et al., 1998). The rolls usually extend from the surface to the capping inversion with a large variety of horizontal sizes from few kilometers to few tens of kilometers. They are characterized by long lifespan of hours or even days as opposed to the short lifespan of the streaks (Drobinski and Foster, 2003). Young et al
65 al (2002) distinguish rolls in narrow mixed-layer rolls, where the ascending air masses are one thermal wide (Weckwerth et al., 1999) and wide mixed-layer rolls, where multiple thermals are grouped within each ascending area (Brümmer, 1999). As Young et al (2002) stated, both types of rolls can be distinguished visually, with the narrow rolls having the form of a "string of pearls" whereas the wide rolls look like a "band of froth".

Remote sensors are exceptionally useful for the identification of coherent ~~turbulent~~ structures. Their ability to scan
70 large areas in a short period is advantageous compared to in situ measurements (Kunkel et al., 1980). Lhermitte (1962), Browning & Wexler (1968) were the first to implement the velocity azimuth display (VAD) technique, also known as plan position indicator (PPI) method, using Doppler radars. The PPI technique provides conical scans or even horizontal surface

75 scans with the appropriate combination of elevation and azimuth angles. Kropfli & Kohn in 1978 were able to study horizontal roll structures by using a dual-Doppler radar in order to observe the wind field in the three dimensions. Several studies followed for different type of radars with more efficient configurations (Kelly, 1982; Lohou et al., 1998; Reinking et al., 1981). Weckwerth et al. (1999) were able to study the evolution of horizontal convective rolls by combining Doppler radar observations with meteorological measurements, radiosondes, flight measurements and satellite images.

80 In recent years, various studies have been carried out by using lidars only. It has been well established that the PPI method can also be applied to Doppler lidars (Cariou et al., 2007; Vasiljević et al., 2016) with the possibility to compute the mean wind profile by using a modified version of the VAD method as it has been demonstrated in the studies of Banta et al., (2002) and Chai et al., (2004). Depending on the selected scanning method of the Doppler lidar it is possible to observe coherent ~~turbulent~~ structures in the atmospheric surface layer (Drobiniski et al., 2004) as well as in the mixed-layer (Drobiniski et al., 1998). Newsom et al. (2008) and Iwai et al. (2008) introduced the dual-Doppler lidar method and revealed its benefits in the observation of coherent ~~turbulent~~ structures. This method was further improved by Träumner et al. (2015) using an 85 optimized dual-Doppler technique. They were able to identify different type of ~~turbulent~~ structures including elongated areas resembling turbulent streaks. They combined quantitative characteristics of the coherence such as the integral scales and the anisotropy coefficients, obtained by a two-dimensional autocorrelation algorithm, a two-dimensional autocorrelation function with the visual observation of the scans ~~by eye~~. However, the subjective classification by observing the images is a time-consuming approach and non-systematic. Furthermore, the use of two Doppler lidars is limited to the institutes that can afford 90 such a high cost and collaborations on short-term campaigns. A much less expensive approach, and suitable for long periods, is to detect the passage of ~~turbulent~~ structures on sonic anemometer time series. For instance, Barthlott et al. (2007), analysed 10 months of data from a meteorological tower located in the surface layer 20 km south of Paris, France and they observed coherent ~~turbulent~~ structures for 36% of the cases. However, their study is limited to point measurements instead of a larger wind field that it is possible to observe via a lidar.

95 This study aims to identify the medium-to-large fluctuations and coherent ~~turbulent~~ structures (mlf-cs) on single Doppler lidar horizontal scans and develop an automatic classification process based on the combination of texture analysis and a supervised machine learning technique, namely the Quadratic Discriminate Analysis (QDA), in order to handle large datasets. Texture analysis is an effective way to evaluate the distribution of the values within an image (Castellano et al., 2004). It is widely used in various scientific fields in order to classify images, covering meteorology (Alparone et al., 1990), medical 100 studies (Holli et al., 2010) and forestry (Kavitakire et al., 2006). ~~The structures are determined by combining texture analysis and machine learning technique~~ There is a lack of long-term studies of structures based on lidar observations and the aforementioned automatic classification process can stimulate the interest in this research field. More particularly, it could facilitate the statistical analysis of the physical parameters of the structures, e. g. the structure size as a function of the planetary boundary layer (PBL) height. Furthermore, it will enable us to study the transitions between structures and how these are 105 associated to the atmospheric conditions. Finally, the impact of the structures on pollutants' concentrations could be examined for long-term studies under stable and unstable conditions. ~~The classification method~~ relies on the observations of radial wind speed recorded using a scanning Doppler lidar settled atop a 75 m-high tower in the centre of Paris, during a two-month period in late summer/early fall. Section 2 presents the experimental set up of the study. The methodology for the identification and classification of the ~~turbulent structures-mlf-cs~~ is demonstrated in Section 3~~Section 0~~. Subsequently, the results of the classification for the training ensemble as well as for the whole dataset are displayed in Section 4. Finally, the key points of 110 the paper are summarized in Section 5.

2. Experimental set up

A two-months measurement campaign (04/09-06/11/2014) was carried out ~~in Paris~~ in order to study the exchange processes of ozone and aerosols in the area in the framework of the VEGILOT [VEGétation et ILOT de chaleur urbain (vegetation & urban heat island)] project in the urban area of Paris (Klein et al., 2019). The Leosphere WLS100 Doppler lidar (www.leosphere.com) with a minimum range of observations at 100 m (Figure 1~~Figure 1~~a) was installed atop a 75 m building in the Jussieu Campus, located in the centre of Paris city (Figure 1~~Figure 1~~b) and was used for wind measurements. Table 1 shows the significant lidar properties during the VEGILOT campaign.

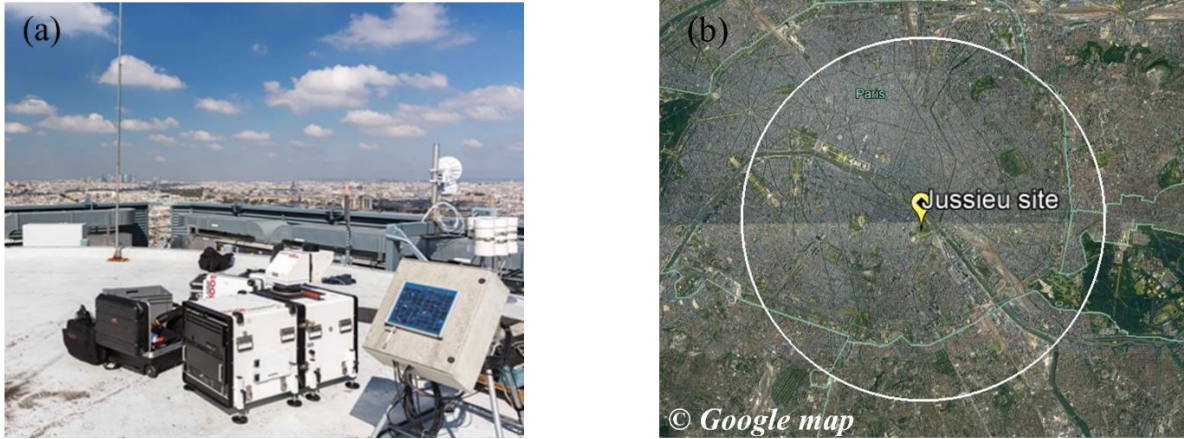


Figure 1: (a) The Doppler lidar installed on the tower roof during the VEGILOT campaign and (b) the measurement site in Paris with the circle of 10 km diameter demonstrating the maximum range of the PPI surface scan (Google earth satellite image).

The Doppler shift frequency between the emitted laser beam and the light backscattered by the aerosols is measured by heterodyne detection associated with Fast Fourier Transform as explained analytically by (Cariou et al., 2007) ~~Kumer et al. (2014) and Veselovskii et al. (2016)~~. A wind lidar is measuring~~The lidar is sensitive only to the radial wind speed i.e. the wind projection along the light beam (counted positive when going away from the lidar).~~

Table 2~~Table 2~~ showcases the implemented scanning methods scanning sequence as it was implemented during the VEGILOT campaign. For the classification of the mlf-cs-turbulent structures, we focused in the current study on the almost horizontal PPI scans (1° elevation angle). During those scans, the lidar emitted beams in azimuth angles from 0° to 360° with for a 2° resolution. This scenario was repeated every 18 minutes hence providing 4577 PPI scans during the whole campaign. The duration of each scan was 3 minutes which is sufficiently fast short for the observation of coherent structures with a lifespan of several minutes. The maximum range of the scans reached 5 km (see white circle of Figure 1~~Figure 1~~b) with a spatial resolution of 50 m. It is noteworthy that the scanning area covers almost exclusively the urban area of Paris. A city famous for regulating the height of the buildings to not exceed 50 m in its' centre (Saint-Pierre et al., 2010). Furthermore, the ground altitude enclosed by the scanning area mostly ranges between 30 to 60 m with the exception of some hills near the boundaries of the scanning range as it can be seen in Figure 2. Therefore, the scanning area can be characterized by a rather homogeneous urban surface. Due to the 1° elevation, the beam was risen by about 87 m between the central point and the point at the 5 km. It was also important for this study to retrieve observations regarding the vertical wind shear. For this purpose, the Doppler beam swinging (DBS) scanning method was implemented. This method was consisted of four line of sight beams at azimuth angles of 0° , 90° , 180° and 270° with an elevation angle of 75° and it was applied twice. The duration of the four beams emission was approximately 15 seconds.

Table 1: Properties of the lidar used for the observation of turbulent structures/mlf-cs

Doppler lidar (Leosphere WLS100)	
Altitude of lidar:	75 m a.g.l.
Minimum range:	100 m
Radial wind speed range:	-30 to 30 m/s

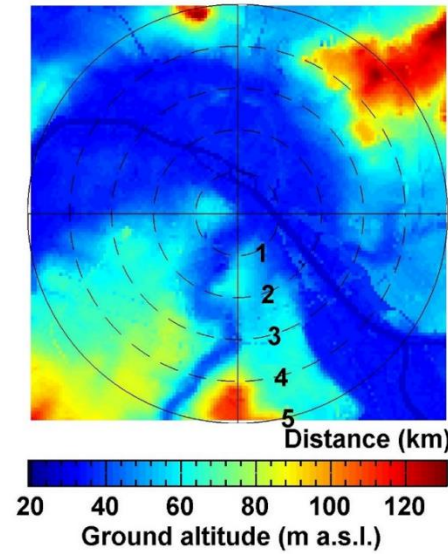
Laser wavelength:	1.543 μm
Radial wind accuracy:	± 0.1 m/s
Accumulation time:	1 sec/beam

180

Table 2: Scanning ~~methods selected~~ ~~sequence~~ during VEGILOT

	Scanning area	Purpose	Elevation & azimuth angle	Scan duration
Plan Position Indicator (PPI)	Almost horizontal scans near surface	Identification of structures	Elevation 1° , azimuth 0 to 360° with 2° resol.	3 min
Doppler Beam Swinging (DBS)	Combination of LOS	Identification of low level jet cases	Elevation 75° & 90° , azimuth 0° , 90° , 180° & 270°	2 x 15 sec

185

Figure 2: Ground altitude map above sea level for the scanning area in Paris.

3. Preparation of the dataset for the classification

3.1 Turbulent radial wind fields

Assuming a homogeneous wind field for horizontal PPI scans, the radial wind measurements u_r taken for the different beams at a given distance from the lidar should follow a cosine function of the azimuth angle, due to the projection of the wind along the beam direction (Eberhard et al., 1989). For instance, the observations at 2 km from the lidar (black ring on [Figure 3a](#) [Figure 2a](#)) are displayed on [Figure 3](#) [Figure 2\(b\)](#) and can be fitted by a cosine function in the form of Eq. (1)(+):

$$u_r = a + b \cos(\theta - \theta_{max}) \quad (1)$$

where b is the mean wind speed, θ_{max} is the wind direction, θ is the azimuth angle of the beam and a is the offset (Browning and Wexler, 1968; Lhermitte, 1962). It is noteworthy that the value of a is much smaller than b for our data. It is possible to retrieve the mean wind from all the “rings” and subsequently calculate the mean wind projected on the beam direction which

195

is displayed on [Figure 3 Figure 2\(c\)](#). The difference between the radial wind field u_r ([Figure 3 Figure 2a](#)) and the mean wind projected on the beam direction ([Figure 3 Figure 2c](#)) is the **turbulent component mlf-cs** of the radial wind field u'_r ([Figure 3 Figure 2d](#)). A parameter that indicates the existence of a turbulent atmosphere. For this study, the radial wind speed values for which the carrier-to-noise ratio is lower than -27dB ($CNR < -27dB$) were disregarded since they were anomalously high, exceeding the values of the rest of the radial wind field by two times or more. Therefore the effective scanning range showcased in [Figure 3](#) is approximately 3 km. For a better visual representation of the patterns, the sign of the u'_r in the current study is positive when the radial wind speed is stronger than the mean wind speed and negative when it is weaker as it is illustrated in the sign convention of [Figure 3 Figure 2\(b\)](#) and it was computed by the following expression:

$$u'_r = |u_r(\theta)| - |f(\theta)| \quad (2)$$

where f is the fitted curve.

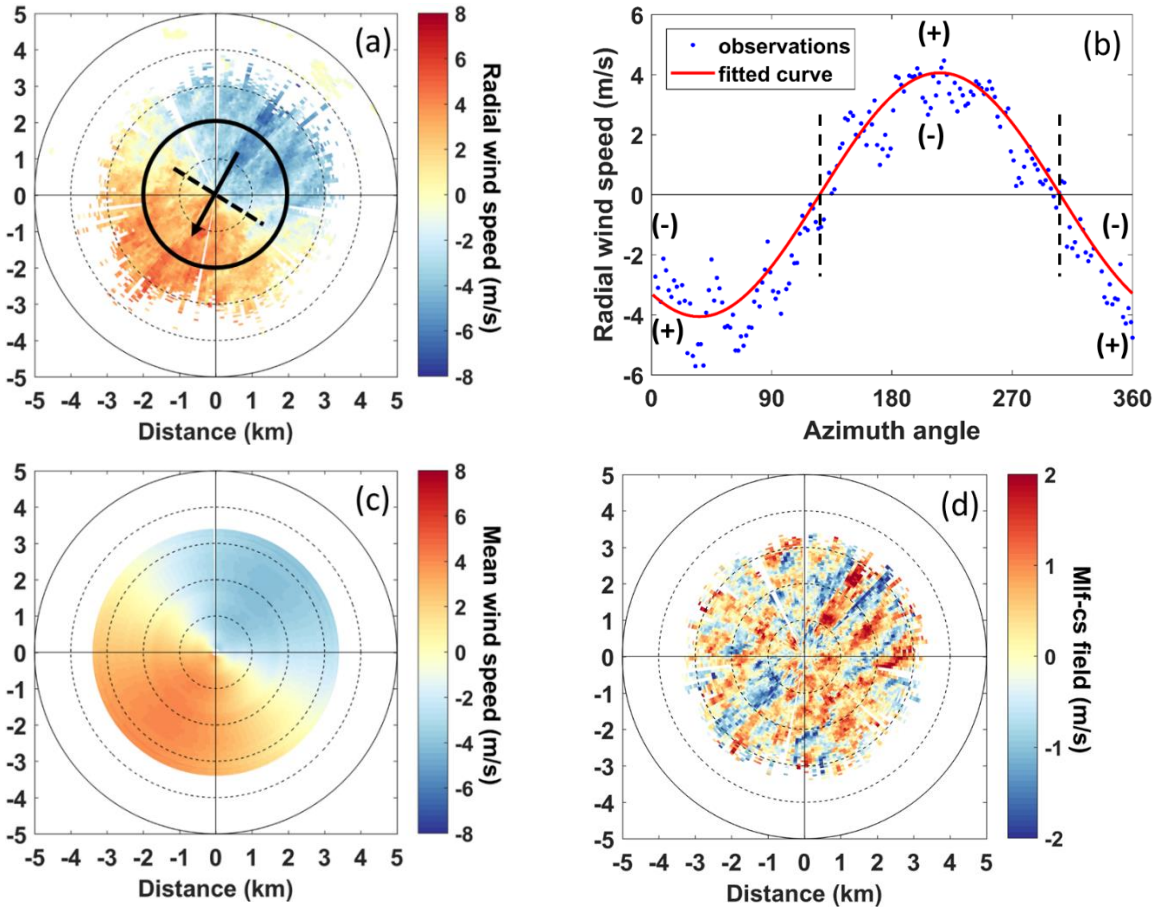


Figure 32: Observations recorded during a quasi-horizontal PPI scan on 08/09/2014 in Jussieu site, Paris at 09:26 UTC. (a) Radial wind speed along with the mean wind direction (black line) and the transverse direction perpendicular to it (black dotted line). (b) Radial wind speed (blue dots) as a function of the azimuth angle at a fixed 2 km distance from the lidar (black circle on panel a) along with the cosine fit function (red line). (c) Mean wind speed projected on the beam direction. (d) **Turbulent component of the radial wind-mlf-cs** field.

The Jussieu site is located in an urban area nearby hills, hence the surface roughness or the orography can affect the regional wind flow **homogeneity of the wind field**. Troude et al. (2002) and Lemonsu and Masson (2002) have performed numerical weather simulations in the area of Paris and have observed that during low wind conditions (below 3 m/s) the orographic effect and the urban heat island effect could be the main drivers for the local wind speed. As a result, in some cases the radial wind field does not follow a cosine function, and therefore the VAD method cannot be applied. This is apparent especially at night when low winds (below 2 m/s) do not have a defined direction (Wilson et al., 1976). [Figure 4 Figure 3](#) presents a case where the radial wind field is not homogeneous. The radial wind speed values e.g. at 2 km did not follow a cosine function ([Figure 4 Figure 3b](#)).

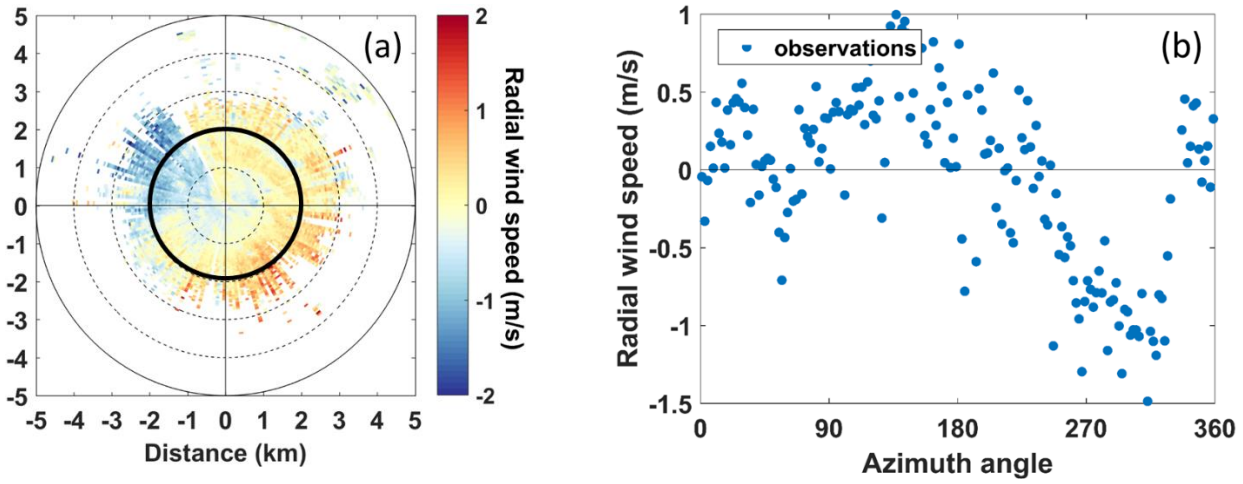


Figure 43: **Aa** case when the VAD method cannot be applied: (a) Radial wind field on 25/09/2014 at 23:42 UTC and (b) Radial wind speed (blue dots) as a function of the azimuth angle at a fixed 2 km distance from the lidar (black circle on panel a).

220 The visual examination of the turbulent radial wind mlf-cs fields led to the identification of three types of remarkable turbulent mlf-cs patterns. The first type was represented by large elongated areas of positive turbulent radial wind mlf-cs accompanied by large elongated areas of negative turbulent radial wind mlf-cs aligned with the mean wind (Figure 5Figure 4a) during the day. In the atmosphere, these types of patterns are encountered concurrently with the existence of rolls, where strong descending motions enhance the horizontal wind speed and descending motions reduce it. The second type of pattern was characterized by large enclosed areas of positive radial turbulent wind mlf-cs field attached to large enclosed areas of negative turbulent wind mlf-cs field (Figure 5Figure 4b) during the day. The convergence zones formed between the positive and negative turbulent wind mlf-cs fields during unstable conditions (e.g. high solar radiation) are able to form strong unaligned thermals. Finally, the third type of pattern consisted of narrow elongated areas alternating between positive radial turbulent wind mlf-cs and negative aligned with the mean wind (Figure 5Figure 4c). These patterns resemble turbulent streaks as they are described in Section 1.

235 In order to train the classification algorithm (Section 4.1), it was necessary to build an ensemble of cases for which the presence of rolls, unaligned thermals or streaks was confirmed by other observations than the lidar measurements. Moderate resolution imaging spectroradiometer (MODIS) true colour images were used to detect the presence of cloud streets over Paris (Figure 5Figure 4d) which confirmed the existence of rolls as stated in Section 1. Close to the moment when the cloud streets were present, rolls patterns were observed at the turbulent radial fields (Figure 5Figure 4a). It is noteworthy to mention that, for the training ensemble, we selected only cases of rolls occurring around the satellite overpass time to ensure the presence of cloud streets and thus the existence of rolls. However, for this classification we are interested in all the cases of rolls, with or without the formation of cloud streets. It is important to note that we observed the occurring patterns near the surface, hence near the lower part of the rolls. Regarding unaligned thermals, solar radiation measurements from the meteorological station of Paris-Montsouris indicated the occasions when the hourly values were higher than the monthly average hourly values according to the Photovoltaic Geographical Information System (Huld et al., 2012) signifying fair cumuli weather conditions. For approximately the same time of the day, we observe the unaligned thermals patterns. Figure 5 Figure 4(b) showcases an example of a turbulent radial wind field with unaligned thermals along with fair weather cumuli over Paris as observed on MODIS true colour image at approximately the same time (Figure 5Figure 4e).

245 Finally concerning streaks, a driving factor for their formation is the existence of a strong wind shear near the surface. The observation of the horizontal wind profiles from the DBS scans revealed when the wind shear was higher than 2 m/s^{-1} , which is defined as the threshold for nocturnal low level jet events (Stull, 1988) (Figure 5Figure 4f). The horizontal wind speed U_{hor} was estimated by the zonal u and meridional v winds via the expression:

$$U_{hor} = \sqrt{u^2 + v^2} \quad (32)$$

Consequently, the wind shear was estimated from the vertical profile of U_{hor} , by subtracting the local minima from the local maxima above it, near the surface. For the training ensemble, for many cases, the wind shear was accompanied by turbulent only night cases when streaks patterns (Figure 5Figure 4c) were accompanied by wind shear higher than 2 s^{-1} were selected so or the training ensemble, only night cases of streaks were selected to ensure that wind shear was the primary factor for the generation of turbulence. In total, 30 cases of each structure type were selected for the training ensemble with an extra category representing all the patterns that are not classified in the other three categories, such as chaotic patterns or cases when the VAD method cannot be applied (Figure 4Figure 3). Regarding rolls, streaks and thermals, only cases with symmetric radial wind fields were selected in order to ensure that the VAD method was applicable.

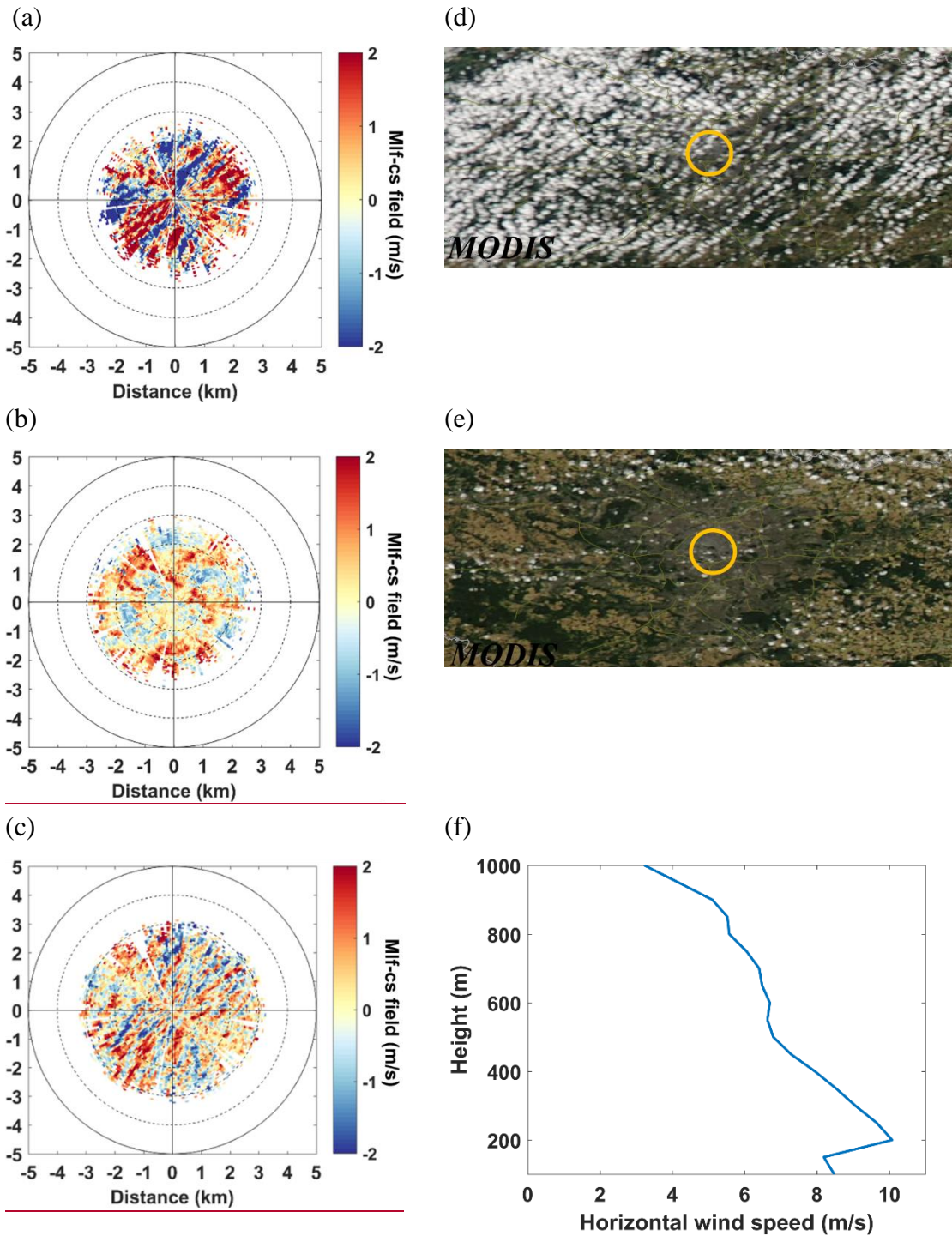


Figure 54: The upper part shows the three types of remarkable turbulent radial wind mlf-cs fields to classify: (a) rolls observed on 13/10/2014 at 12:52 UTC, (b) unaligned thermals observed on 16/09/2014 at 12:52 UTC and (c) streaks observed on 09/09/2014 at 20:49 UTC. The lower part shows the ancillary observations used to ascertain the turbulence structure pattern type: (d) and (e) true color image recorded by MODIS Aqua on the same day as (a) and (b) at 12:50 UTC, (f) horizontal wind speed profile recorded by the Doppler lidar using the DBS technique on the same day as (c) at 20:51 UTC.

3.2 Computation of the co-occurrence matrices

In order to retrieve comparable texture analysis parameters from the **turbulent wind mlf-cs** field of the scans, the **radial turbulent wind mlf-cs** field was rotated so that the mean wind direction was aligned to the vertical (0° corresponds to a wind blowing from the North). Then, the coordinates were converted from polar to Cartesian. It was also important to adjust the contrast of the image so that the difference between the areas of positive and negative turbulent wind speed became more prominent. For this purpose, the contrast of the images was increased by mapping the turbulent wind speed values into eight levels. One bin included all the negative values below -0.5 m/s, six bins were equally distributed between -0.5 m/s and $+0.5$ m/s and one bin included all the positive values above $+0.5$ m/s (Figure 6 Figure 5b).

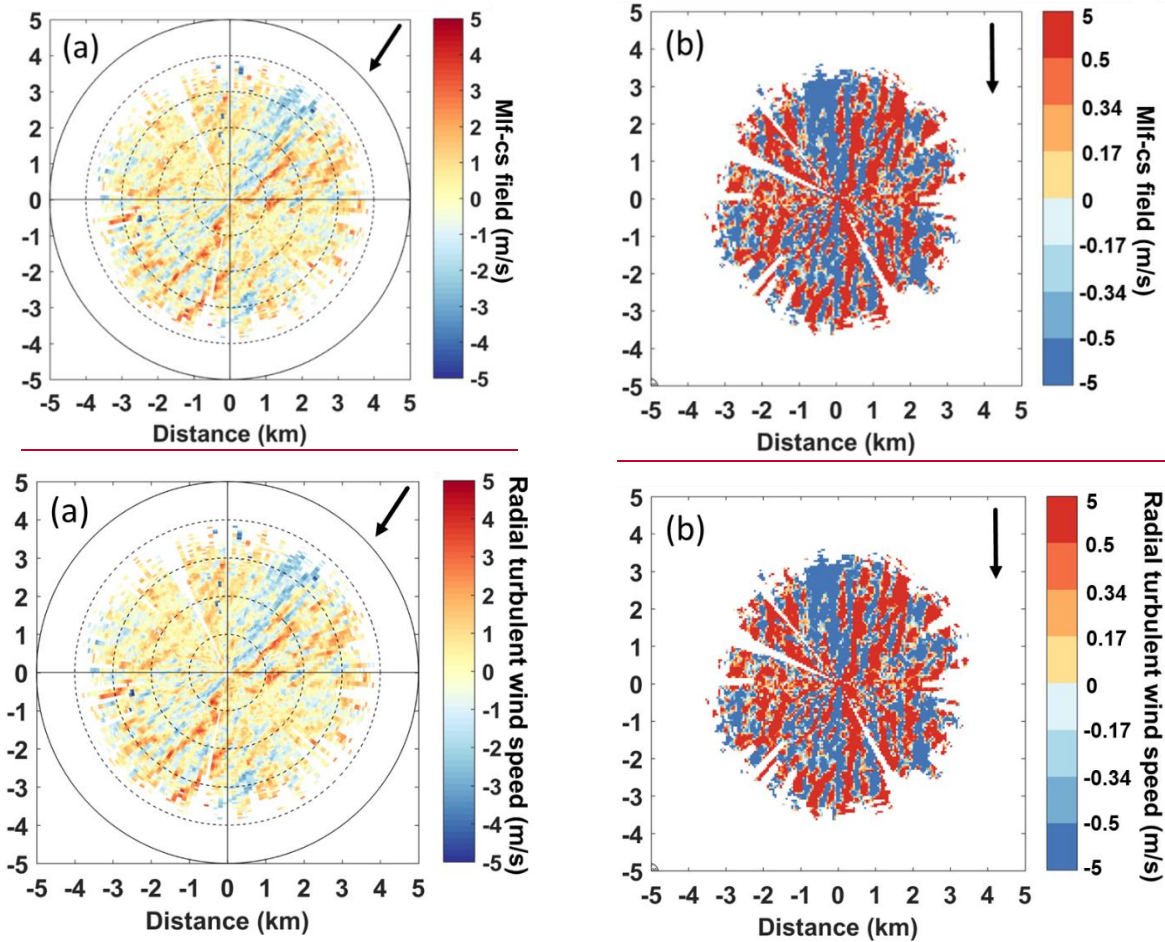


Figure 65: The **radial turbulent wind mlf-cs** field (a) before and (b) after image pre-processing with the arrow representing the mean wind direction on 10/09/2014 at 19:57.

For the automated classification of patterns, we need to map them to a space of corresponding numerical parameters. Each reconstructed **turbulent wind mlf-cs** field is represented by a matrix (cells corresponds to pixels) from which 8×8 co-occurrence matrices (CM) can be constructed (Haralick et al., 1973). The rows and columns of the CM represent the wind levels from 1 to 8, whereas the cells contain the **frequency of the combination of two neighbour pixels in the image number of occurrences of neighbour pairs with values corresponding to the row and column index**. More specifically, the element at line i and column j contains the number of pixels with value i which are neighboured by pixels with value j . The first neighbour can be searched at different direction (e.g. left-right, up-down or diagonally) defining the cell pair orientation. In the same way a second, a third, etc. neighbour can be selected. Thus, the CM can be calculated for any cell pair orientations and neighbour order. CM were computed for various distances, i.e. neighbour orders n from 1 to 30 (distance from 50 m to 1.5 km) and all possible cell pair orientations, i.e. azimuth angles φ from -90° (transverse direction from the mean wind in the counter clockwise direction) to $+90^\circ$ (transverse direction in the clockwise direction). Table 3 Table 3 shows the cell values of the CM built from the image of Figure 6 Figure 5(b) for the first neighbour ($n = 1$) and for a cell pair aligned with the mean wind and

340 oriented in the same direction (azimuth $\varphi = 0^\circ$). It is apparent that the vast majority of the occurrences are concentrated in the cells [1,1] and [8,8] as the structures are elongated and aligned with the mean wind direction.

Table 3: Co-occurrence matrix after the image pre-processing (Figure 6 Figure 5b) for the first neighbour ($n = 1$) and for a cell pair aligned with the mean wind and oriented in the same direction (azimuth $\varphi = 0^\circ$).

	1	2	3	4	5	6	7	8
1	3065	226	164	118	113	57	35	94
2	255	67	77	58	36	26	23	48
3	181	81	59	61	44	51	35	72
4	133	58	63	91	71	50	40	92
5	98	51	59	65	67	63	58	154
6	58	36	50	53	75	72	78	169
7	46	30	38	53	60	61	55	231
8	73	45	78	104	151	201	246	3402

345 Table 4: Co-occurrence matrix after the image pre-processing (Figure 6 Figure 5b) for the third neighbour ($n = 3$) and for the transverse direction in the clockwise direction (azimuth $\varphi = +90^\circ$).

	1	2	3	4	5	6	7	8
1	1497	231	203	182	165	168	170	1149
2	185	19	25	43	27	27	25	200
3	183	29	26	29	33	31	21	207
4	195	32	37	39	29	31	28	185
5	203	29	38	31	36	31	26	208
6	201	26	25	25	26	39	29	198
7	175	27	23	26	32	21	37	212
8	1063	179	187	196	243	206	217	1719

On the other hand, Table 4 Table 4 shows the CM of Figure 6 Figure 5(b) for the third neighbour ($n = 3$) and for a cell pair oriented perpendicularly to the mean wind (transverse direction) with a clockwise rotation (azimuth angle $\varphi = +90^\circ$). In this case, the occurrences have been distributed to the cells [1,1] and [8,8], as well as to the cells [1,8] and [8,1]. As we can see on Figure 6 Figure 5(b), the structures alternate between positive and negative values in the direction transverse to the mean wind, thus creating this difference in the CM compared to Table 3 Table 3.

3.3 Texture analysis parameters for the classification of the turbulent structures

355 It is possible to compute several texture analysis parameters from each CM. Srivastava et al. (2018) were able to distinguish different synthetic patterns by using four texture analysis parameters: correlation, contrast, homogeneity and energy. Correlation indicates the existence of linear structures in the image, with high values associated to a large amount of linear structure in the image. Contrast reveals the local variations in an image, where a large amount of variations leads to high values. Homogeneity is self-explanatory and the high values represent a homogeneous image. Finally, energy measures the uniformity of an image with the highest values corresponding to constant or periodic forms (Haralick et al., 1973; Yang et al., 2012). In their study, the striped patterns resemble the elongated patterns of streaks and rolls that we observe in the radial

turbulent wind field. Therefore, the same texture analysis parameters were selected for calculation in our dataset. More particularly, these parameters were computed by the Eq. ~~(4)(2)~~, ~~(5)(3)~~, ~~(6)(4)~~ and ~~(7)(5)~~:

Homogeneity:
$$Hom(\varphi, n) = \sum_{i,j} \frac{p(i,j)}{1 + |i - j|} \quad (42)$$

Contrast:
$$Con(\varphi, n) = \sum_{i,j} p(i,j)|i - j|^2 \quad (53)$$

Correlation:
$$Cor(\varphi, n) = \sum_{i,j} \frac{(i - \mu_i)(j - \mu_j)p(i,j)}{\sigma_i \sigma_j} \quad (64)$$

365

Energy:
$$En(\varphi, n) = \sum_{i,j} p(i,j)^2 \quad (75)$$

where $p(i,j) = \frac{CM(i,j)}{\sum_{i,j} CM(i,j)}$ for the i, j position in the CM, marginal expectations $\mu_i = \sum_i \sum_j i \cdot p(i,j)$, $\mu_j = \sum_i \sum_j j \cdot p(i,j)$ and the marginal standard deviations $\sigma_i = \sqrt{\sum_i \sum_j (i - \mu_i)^2 \cdot p(i,j)}$, $\sigma_j = \sqrt{\sum_i \sum_j (j - \mu_j)^2 \cdot p(i,j)}$.

370

At a given neighbour order n , it is then possible to study the dependence of the texture parameters to the azimuth angle φ (see an example of such a dependence on ~~Figure 7~~~~Figure-6~~). The streaks and rolls have a more prominent peak in the longitudinal direction ($\varphi = 0^\circ$) compared to the unaligned thermals and “others” patterns. As streaks and rolls are aligned with the mean wind (azimuth $\varphi = 0^\circ$), those peaks result from the elongated shapes of these patterns.

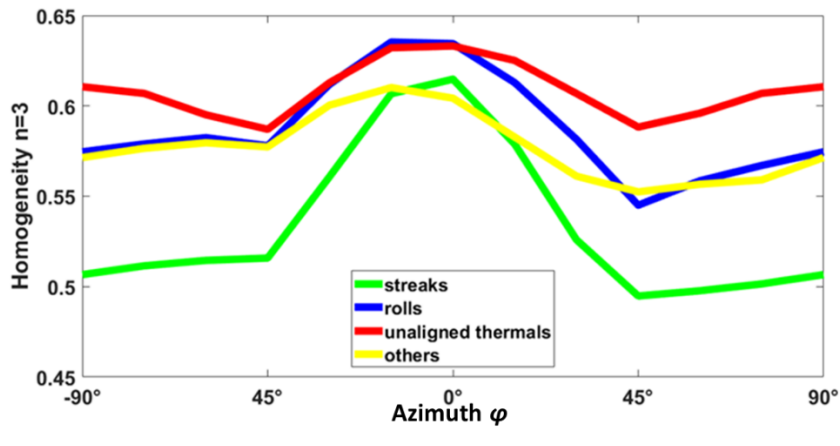


Figure 76: Third neighbour homogeneity as a function of azimuth for one selected scan of each type.

375

Three parameters of the curve in ~~Figure 7~~~~Figure-6~~ were selected in order to distinguish the different types of structures. For instance, for the homogeneity curves, these parameters are defined by the Eq. ~~(8)(6)~~, ~~(9)(7)~~ and ~~(10)(8)~~:

Amplitude:
$$Hom. Amp(n) = \max_{\varphi} (Hom(\varphi, n)) - \min_{\varphi} (Hom(\varphi, n)) \quad (86)$$

Integral:
$$Hom. Int(n) = \sum_{\varphi} Hom(\varphi, n) \quad (97)$$

Symmetry:
$$Hom. Sym(n) = \sum_{\varphi} |Hom(\varphi, n) - Hom(-\varphi, n)| \quad (108)$$

380 These three curve parameters were calculated for the four texture analysis parameters and for each of the thirty
neighbour orders, which gives 360 parameters. In addition to these parameters, the UTC hour (close to solar time in Paris), the
average mean wind speed and the root-mean-square error of the cosine fit (~~Figure 3~~~~Figure 2b~~) were included in the classification
parameters. The total number of classification parameters associated with each scan was therefore 363.

4. Classification using supervised machine learning

4.1 Algorithm training and classification error

385 In order to classify the ~~turbulent structures-mlf-cs~~ according to the aforementioned texture analysis parameters, the
supervised machine learning methodology was applied (Bonamente, 2017; James et al., 2000; Kubat, 2017). The ~~Quadratic~~
~~Discriminant Analysis (QDA)~~ algorithm was used, that minimizes the total error probability of the classification, assuming
that features of each class have a multidimensional Gaussian distribution. ~~QDA or normal Bayesian classification~~ (Hastie et
al., 2009) ~~is the parametric approach implying that probability density functions (PDF) belong to the family of normal~~
390 ~~distributions. It is a classical algorithm of the supervised machine learning, based on the principle of maximum likelihood. The~~
~~general idea is to estimate the PDF for each class, and then select the most probable class~~ (Kubat, 2017).

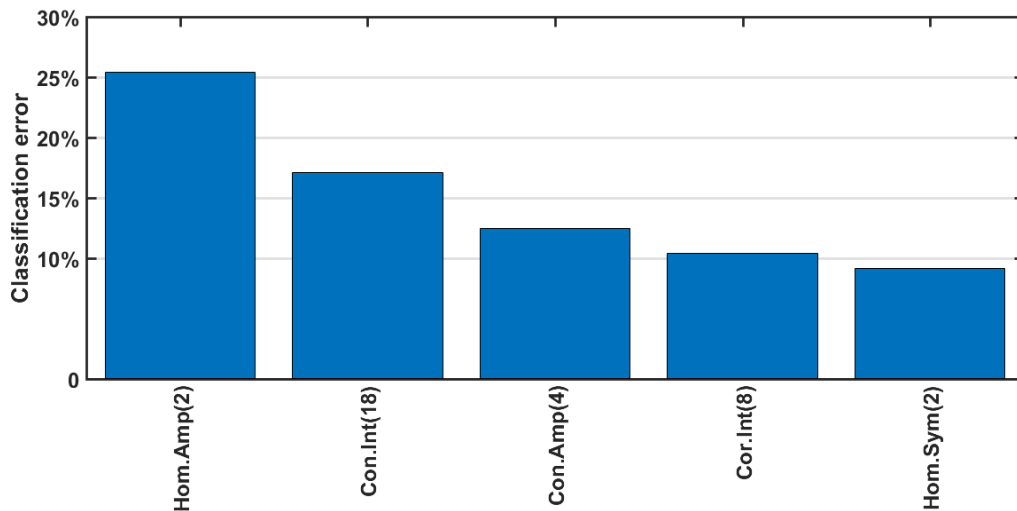
~~The greedy algorithm of stepwise forward selection was used in the article, which is the standard and frequently used~~
~~method of reduction of the feature space. As indicated in (Sokolov et al., 2020), it can be formulated as follows. The features~~
~~are divided into two groups - accepted in the classification model and remaining, for which an estimate of the possibility of~~
395 ~~acceptance into the model is checked. Features from the set of “remains” are consecutively added to the model and~~
~~corresponding estimations of the classification error are calculated. From the received set of errors, the minimum is chosen~~
~~and compared with the error of the previous model. If a significant reduction of the error occurred, then the corresponding~~
~~feature is accepted into the model, if not then the process stops.~~ The QDA was trained (Hastie et al., 2009; Sokolov et al.,
2020) with the 150-case ensemble described in Section 3.1: 30 cases of streaks, 30 cases of rolls, 30 cases of unaligned thermals
400 and 60 cases of “others”. The category of “others” was represented by twice more cases since it is expected to be the dominant
category in the classification, as it includes the chaotic ~~radial turbulent wind-mlf-cs~~ fields and the cases where the ~~turbulent~~
~~wind-mlf-cs~~ field was not computed successfully by the VAD method. ~~The algorithm can be sensitive to an unbalanced training~~
~~ensemble. Therefore, the selection of a training ensemble based on the expected results was preferred~~ (Kubat, 2017).

The classification error of the QDA technique could be estimated for the training ensemble by means of the 10-fold
405 cross validation. In this method, the algorithm is trained using 90% of the training ensemble (135 cases), then it is applied to
the remaining 10% (15 cases) and the resulting (output) classes are compared to the expected (target) classes. The process is
repeated 10 times, each time extracting a different 10% sample for test, until the entire training ensemble has been tested.

As the number of dimensions of the feature space (363) was significantly higher than the number of patterns of the
training ensemble (150), the application of all the features leads to the curse of the dimensionality problem, when the
410 classification works well only for the training data and fails for the test set. In order to deal with this problem, we reduced the
feature space by selecting the most informative components using the stepwise forward selection algorithm (Sokolov et al.,
2020). The resulting sequence of these components and the decrease of the 10-fold cross validation classification error are
presented in ~~Figure 8~~~~Figure 7~~. The classification error reached a minimum of about 9.2% when five parameters were used;
taking more into account increased the classification error.

415 ~~Analytically, these parameters are the amplitude of the 2nd-neighbour homogeneity curve, the integral of the 18th-~~
~~neighbour contrast curve, the amplitude of the 4th-neighbour contrast curve, the integral of the 8th-neighbour correlation curve~~
~~and the symmetry of the 2nd-neighbour homogeneity curve. These results show that the prominent peaks are a distinctive~~
~~characteristic for the elongated patterns as the amplitude of the homogeneity and contrast curves are two of the significant~~
~~parameters. Furthermore, the integral or more precisely the sum of the points of the curves for the contrast and for the~~

420 correlation curves are significant parameters as well. This is important especially for the distinction between the categories
 425 thermals and “others” as their amplitude may not differ substantially since the patterns are not towards a specific direction, yet
 a chaotic area will have higher values of contrast and lower values of correlation compared to an enclosed homogeneous area.
 Finally, the symmetry of the homogeneity curve as a classifier reveal the urgency to align the radial turbulent wind fields to
 the mean wind direction and thus align the structures such as streaks and rolls with the mean wind direction in order to be
 distinguishable from the random positions of the enclosed structures of the thermals or the chaotic structures of the “others”.
 It is also crucial to note that the parameters cover various distances, from the 2nd-neighbour, which in grid points is 100 m to
 the 18th-neighbour which is 900 m. This is necessary for our classification since streaks and rolls are both elongated patterns
 but their transverse horizontal sizes differ. In particular, these parameters were the amplitude and symmetry of the homogeneity
 curve, the integral and the amplitude of the contrast curve and the integral from the correlation curve. As explained in Section
 0, elongated structures show a more prominent peak in the homogeneity (or the opposite for contrast) curve and as a result,
 they are characterized by a higher amplitude compared to unaligned thermals and “others” patterns. Similarly, the values of
 the integral of the curves with prominent peaks differentiate from quasi-constant curves that occur for patterns with large
 enclosed areas (thermals) or for chaotic ones (“others”). The significant parameters cover various distances from the 2nd
 neighbour (100 m) to the 18th (900 m), hence- Furthermore it demonstrates the ability of the algorithm to distinguish
 435 structures with different sizes. It is noteworthy that the curve parameters play a more significant role in the classification of
 the structures in comparison to time, mean wind field and cosine fit RMSE.



440 Figure 87: Texture analysis parameters selected to minimize the classification error of the training ensemble by the QDA method.
 From left to right: Amplitude of the homogeneity for the 2nd-neighbour, integral of the contrast for the 18th-neighbour, amplitude of
the contrast for the 4th-neighbour, integral of the correlation of the 8th-neighbour and symmetry of the homogeneity for the
2ndneighbour.

445 The detailed results of the cross-validation of QDA classification for the algorithm with five predictors are
 displayed in Table 5. The algorithm allowed classifying correctly about 91% of the training ensemble. The
 algorithm performs the most precise classification for the streaks with a classification error of only 3.3% as one case
 was misclassified as rolls. Regarding the category “others”, the results are equivalently accurate with a classification
 error of 3.3% as two cases were misclassified as thermals. Moreover, the performance of the algorithm for rolls was
 good with a classification error of 10% with 3 cases were misclassified as thermals. Thermals were the most
 troublesome type for classification by the algorithm, the algorithm classified correctly 24 cases. Four cases were
 misclassified as rolls and 2 cases as “others” showing a classification error of 20%.

450

Table 5: Confusion matrix calculated for the training dataset. The “target class” corresponds to the ~~visual eye made~~ classification while the “output class” corresponds to the class attributed by the algorithm. Therefore, the cells in the “roll” column, for instance, give the number of roll cases that were classified properly (roll line) or improperly (other lines) in the different categories.

		Target class				
		Others	Streaks	Rolls	Thermals	
Output class	Others	58 38.7%	0 0.0%	0 0.0%	2 1.3%	96.7% 3.3%
	Streaks	0 0.0%	29 19.3%	0 0.0%	0 0.0%	100.0% 0.0%
Rolls	Others	0 0.0%	1 0.7%	27 18.0%	4 2.7%	84.4% 15.6%
	Thermals	2 1.3%	0 0.0%	3 2.0%	24 16.0%	82.8% 17.2%
		96.7%	96.7%	90.0%	80.0%	92.0%
		3.3%	3.3%	10.0%	20.0%	8.0%

455 4.2 Results of the trained algorithm over the 2-month dataset

The whole dataset, consisting in 4577 scans, was classified according to the five parameters showcased in ~~Figure 8~~ ~~Figure 7~~. The results are displayed in ~~Figure 9~~ ~~Figure 8~~.

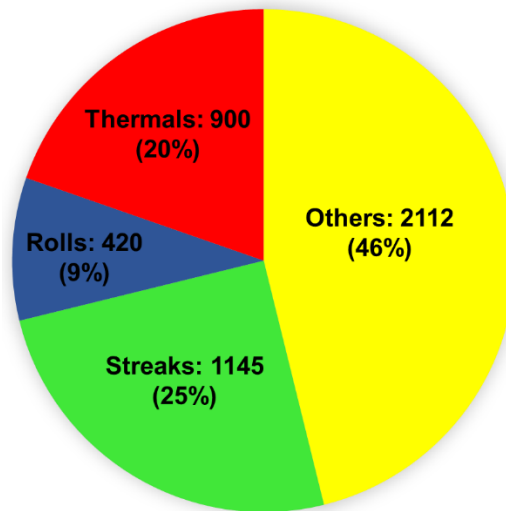
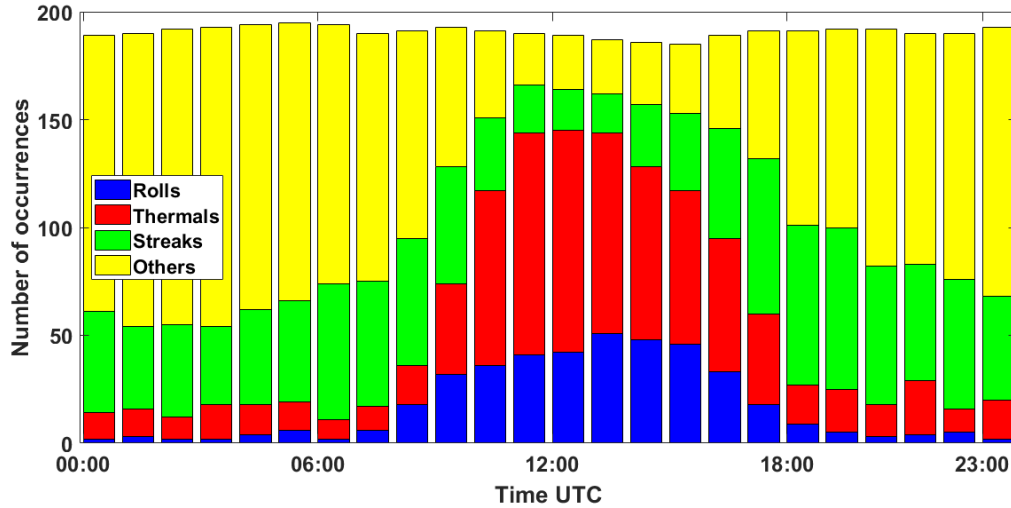


Figure 9: Classification of the whole ensemble using the QDA method according to the parameters of ~~Figure 8~~ ~~Figure 7~~.

460 The algorithm classifies 54% of the two-month dataset as containing ~~turbulent structures mlf-cs~~ and 34% in particular as coherent ~~turbulent~~ structures (streaks, rolls). The most frequent cases of ~~turbulent structures mlf-cs~~ were streaks (25%) and the least frequent were rolls (9%). It is important to note that, in our classification, we consider only thermals and rolls during daytime. ~~Figure 10~~ ~~Figure 9~~ illustrates the number of occurrences for each type of structure at a particular time of the day during the two months of the campaign. It is evident that despite time was ~~not a much less significant one of the selected classifiers~~,
465 ~~the number of occurrences of the structures show a distribution that can be associated to the atmospheric conditions. More particularly, rolls and thermals were mainly classified during day. This result is noteworthy as these structures are linked to a well-developed atmospheric boundary layer during day. On the contrary, compared to the curves parameters, the structures~~

show a time preference. There were scarcely any rolls cases observed at night, though and a few unaligned thermals were classified at night. This stems from the training process, where some cases of thermal were improperly classified as “other” and the reverse. On the contrary “others” cases were mostly observed during the night. This was expected since the cases of low winds with no defined direction –when the VAD method cannot be applied– occur mainly during the night. We also see that streaks were observed more frequently during the night, when mechanical turbulence becomes dominant. This was also expected as the nocturnal low level jets is a main driving factor for the formation of streaks and we observed the occurrence of wind shear higher than 2 s^{-1} over Paris for 20 out of the 62 nights during the VEGILOT campaign.



475 Figure 109: Histogram of the number of occurrences of the different types of structures with respect to time UTC.

5. Conclusions

The current study showcases that it is possible to identify and classify turbulent structures such as streaks, rolls and unaligned thermals with horizontal scans from a single Doppler lidar by combining texture analysis parameters and the QDA supervised machine learning technique. More particularly a two-months campaign in Paris (VEGILOT) provided radial wind speed observation for 4577 horizontal scans with a 1° elevation. By applying the VAD method was used to retrieve to the radial turbulent wind field observations, it is possible to identify mlf-cs that can be distinguished to narrow elongated (streaks), wide elongated (rolls), large enclosed (thermals) and chaotic (“others”) patterns. These diversities of the By analysing patterns of the radial turbulent wind field, it was evident that the elongated patterns (streaks, rolls) showed a prominent peak for were also depicted in the curves of the texture analysis parameters with the elongated patterns (streaks, rolls) showing a prominent peak compared to more chaotic or enclosed patterns (unaligned thermals).

In order to apply the supervised machine learning methodology for the classification of the ensemble, a training ensemble of 150 cases was selected by combining visual examination of the patterns and studying characteristic physical properties corresponding to streaks, rolls and unaligned thermals. For this purpose Subsequently, the QDA algorithm with stepwise forward selection of the features was applied to the training ensemble in and its performance was estimated using the cross-validation technique. The algorithm allowed classifying correctly about results showed a successful classification for 91% of the dataset training ensemble using five texture analysis parameters as predictors. More particularly, these parameters were the amplitude of the 2nd-neighbour homogeneity curve and the amplitude of the 4th-neighbour contrast curve which were associated to the prominent peaks of the elongated patterns (streaks, rolls). Furthermore, the integral of the 18th-neighbour contrast curve and the integral of the 8th-neighbour correlation curve which could distinguish, for example, chaotic patterns (“others”) with high contrast and lower values of correlation between neighbour points compared to an enclosed homogeneous (thermals). Finally, the symmetry of the 2nd-neighbour homogeneity curve revealed the importance to align the mlf-cs fields to the mean wind direction. Another striking outcome of the QDA classification was the variety of the classifiers in terms of

500 distance between the grid points. The 2nd-neighbour translates in a distance between two grid points equivalent to 100 m and for the 18th-neighbour to 900 m. This is essential for the classification between patterns with different sizes such as streaks and rolls.-The algorithm performed best for the category of ~~turbulent~~ streaks with a classification error of only 3.3%. Time, mean wind speed and the cosine fit RMSE of the VAD method were not selected by the algorithm for the classification.

505 The whole ensemble of the 4577 scans was classified by the trained QDA algorithm using the five selected texture analysis parameters. The results showed that 54% of cases were classified as ~~structures-mlf-cs~~ among which 34% were coherent ~~turbulent~~ structures (streaks, rolls). The streaks were mostly observed during night whereas the thermals and rolls were almost exclusively observed during the day, with only a few cases classified between sunset and sunrise. The classified ensemble can be used for statistical studies of the ~~turbulent structures~~ mlf-cs physical parameters, such as structure size as a function of weather conditions (PBL height, temperature, wind speed, radiation etc.). Moreover, the development of the structures can be analysed and comprehended.

510 **Data availability**

All lidar data used in the study are property of the Laboratoire de Physico-Chimie de l'Atmosphere (LPCA), Dunkirk, France and are not publicly available. MODIS satellite images are publicly available following NASAs' open data policy (<https://earthdata.nasa.gov/collaborate/open-data-services-and-software>).

Author contribution

515 IC, EDE, HD and AS conceptualized this study and developed the methodology. HD, PA and MF installed and monitored the instrument on the field. IC processed the data and analysed the results for all parts of the study, with the help of HD, AS and EDM for Section 4. IC wrote the original draft of the manuscript, with contributions from HD, EDE and AS. All authors participated in the review and editing of the manuscript and agreed to this version.

Competing interests

520 The authors declare that they have no conflict of interest.

Acknowledgements

The authors thank F. Ravetta, J. Pelon, G. Plattner and A. Klein of the LATMOS, Sorbonne University, Paris for organizing and carrying out the VEGILOT campaign.

525 This work is a contribution to the CPER research project IReNE and CLIMIBIO. The authors thank the French "Ministère de l'Enseignement Supérieur et de la Recherche", the "Hauts-de-France" Region and the European Funds for Regional Economic Development for their financial support to this project. The work is supported by the CaPPA project. The CaPPA project (Chemical and Physical Properties of the Atmosphere) is funded by the French National Research Agency (ANR) through the PIA (Programme d'Investissement d'Avenir) under contract "ANR-11-LABX-0005-01" and by the Regional Council "Nord-Pas de Calais" and the "European Funds for Regional Economic Development (FEDER).

530 We acknowledge the use of imagery provided by services from NASA's Global Imagery Browse Services (GIBS), part of NASA's Earth Observing System Data and Information System (EOSDIS).

Experiments presented in this paper were carried out using the CALCULCO computing platform, supported by SCoSI/ULCO (Service COmmun du Système d'Information de l'Université du Littoral Côte d'Opale).

This study was funded by RFBR, project number 20-07-00370.

- Adrian, R.J., 2007. Hairpin vortex organization in wall turbulence. *Phys. Fluids* 19, 41301. <https://doi.org/10.1063/1.2717527>
- Alparone, L., Benelli, G., Vagniluca, A., 1990. Texture-based analysis techniques for the classification of radar images. *IEE proceedings. Part F. Commun. radar signal Process.* 137, 276–282. <https://doi.org/10.1049/ip-f-2.1990.0041>
- Aouizerats, B., Tulet, P., Pigeon, G., Masson, V., Gomes, L., 2011. Atmospheric Chemistry and Physics High resolution
540 modelling of aerosol dispersion regimes during the CAPITOUL field experiment: from regional to local scale interactions. *Atmos. Chem. Phys* 11, 7547–7560. <https://doi.org/10.5194/acp-11-7547-2011>
- Banta, R.M., Newsom, R.K., Lundquist, J.K., Pichugina, Y.L., Coulter, R.L., Mahrt, L., 2002. Nocturnal low-level jet characteristics over Kansas during cases-99. *Boundary-Layer Meteorol.* 105, 221–252. <https://doi.org/10.1023/A:1019992330866>
- 545 Barthlott, C., Drobinski, P., Fesquet, C., Dubos, T., Pietras, C., 2007. Long-term study of coherent structures in the atmospheric surface layer. *Boundary-Layer Meteorol.* 125, 1–24. <https://doi.org/10.1007/s10546-007-9190-9>
- Bonamente, M., 2017. *Statistics and Analysis of Scientific Data*. *Grad. Texts Phys.* 55–83. <https://doi.org/10.1007/978-1-4939-6572-4>
- Browning, K.A., Wexler, R., 1968. The determination of kinematic properties of a wind field using Doppler radar. *J. Appl.*
550 *Meteorol.* 7, 105–113. [https://doi.org/10.1175/1520-0450\(1968\)007<0105:tdokpo>2.0.co;2](https://doi.org/10.1175/1520-0450(1968)007<0105:tdokpo>2.0.co;2)
- Brümmer, B., 1999. Roll and cell convection in wintertime Arctic cold-air outbreaks. *J. Atmos. Sci.* 56, 2613–2636. [https://doi.org/10.1175/1520-0469\(1999\)056<2613:RACCIW>2.0.CO;2](https://doi.org/10.1175/1520-0469(1999)056<2613:RACCIW>2.0.CO;2)
- Cariou, J.P., Parmentier, R., Valla, M., Sauvage, L., Antoniou, I., Courtney, M., 2007. An innovative and autonomous 1.5 μm Coherent lidar for PBL wind profiling, in: *Proceedings of 14th Coherent Laser Radar Conference*.
- 555 Castellano, G., Bonilha, L., Li, L.M., Cendes, F., 2004. Texture analysis of medical images. *Clin. Radiol.* <https://doi.org/10.1016/j.crad.2004.07.008>
- Chai, T., Lin, C.-L., Newsom, R.K., 2004. Retrieval of Microscale Flow Structures from High-Resolution Doppler Lidar Data Using an Adjoint Model, *Journal of the Atmospheric Sciences*. American Meteorological Society. [https://doi.org/10.1175/1520-0469\(2004\)061<1500:ROMFSF>2.0.CO;2](https://doi.org/10.1175/1520-0469(2004)061<1500:ROMFSF>2.0.CO;2)
- 560 Chin-Hoh Moeng, Sullivan, P.P., 1994. A comparison of shear and buoyancy-driven planetary boundary layer flows. *J. Atmos. Sci.* 51, 999–1022. [https://doi.org/10.1175/1520-0469\(1994\)051<0999:acosab>2.0.co;2](https://doi.org/10.1175/1520-0469(1994)051<0999:acosab>2.0.co;2)
- Drobinski, P., Brown, R.A., Flamant, P.H., Pelon, J., 1998. Evidence of organized large eddies by ground-based Doppler lidar, sonic anemometer and sodar. *Boundary-Layer Meteorol.* 88, 343–361. <https://doi.org/10.1023/A:1001167212584>
- Drobinski, P., Carlotti, P., Newsom, R.K., Banta, R.M., Foster, R.C., Redelsperger, J.-L., 2004. The structure of the near-
565 neutral atmospheric surface layer. *J. Atmos. Sci.* 61, 699–714. [https://doi.org/10.1175/1520-0469\(2004\)061<0699:TSOTNA>2.0.CO;2](https://doi.org/10.1175/1520-0469(2004)061<0699:TSOTNA>2.0.CO;2)
- Drobinski, P., Foster, R.C., 2003. On the origin of near-surface streaks in the neutrally-stratified planetary boundary layer. *Boundary-Layer Meteorol.* 108, 247–256. <https://doi.org/10.1023/A:1024100125735>
- Eberhard, W.L., Cupp, R.E., Healy, K.R., 1989. Doppler lidar measurement of profiles of turbulence and momentum flux. *J.*
570 *Atmos. Ocean. Technol.* 6, 809–819. [https://doi.org/10.1175/1520-0426\(1989\)006<0809:dlmopo>2.0.co;2](https://doi.org/10.1175/1520-0426(1989)006<0809:dlmopo>2.0.co;2)
- Haralick, R.M., Dinstein, I., Shanmugam, K., 1973. Textural features for image classification. *IEEE Trans. Syst. Man Cybern.* SMC-3, 610–621. <https://doi.org/10.1109/TSMC.1973.4309314>
- Hastie, T., Tibshirani, R., Friedman, J., 2009. *The elements of statistical learning: Data mining, inference, and prediction*, Springer Series in Statistics.
- 575 Holli, K., Lääperi, A.L., Harrison, L., Luukkaala, T., Toivonen, T., Ryymin, P., Dastidar, P., Soimakallio, S., Eskola, H., 2010. Characterization of Breast Cancer Types by Texture Analysis of Magnetic Resonance Images. *Acad. Radiol.* 17, 135–141. <https://doi.org/10.1016/j.acra.2009.08.012>

- Huld, T., Müller, R., Gambardella, A., 2012. A new solar radiation database for estimating PV performance in Europe and Africa. *Sol. Energy* 86, 1803–1815. <https://doi.org/10.1016/j.solener.2012.03.006>
- 580 Hussain, A.K.M.F., 1983. Coherent structures - Reality and myth. *Phys. Fluids* 26, 2816–2850. <https://doi.org/10.1063/1.864048>
- Hutchins, N., Marusic, I., 2007. Evidence of very long meandering features in the logarithmic region of turbulent boundary layers. *J. Fluid Mech.* 579, 1–28. <https://doi.org/10.1017/S0022112006003946>
- Iwai, H., Ishii, S., Tsunematsu, N., Mizutani, K., Murayama, Y., Itabe, T., Yamada, I., Matayoshi, N., Matsushima, D.,
585 Weiming, S., Yamazaki, T., Iwasaki, T., 2008. Dual-Doppler lidar observation of horizontal convective rolls and near-surface streaks. *Geophys. Res. Lett.* 35, L14808. <https://doi.org/10.1029/2008GL034571>
- James, G., Witten, D., Hastie, T., Tibshirani, R., 2000. An introduction to Statistical Learning, Current medicinal chemistry. <https://doi.org/10.1007/978-1-4614-7138-7>
- Kayitakire, F., Hamel, C., Defourny, P., 2006. Retrieving forest structure variables based on image texture analysis and
590 IKONOS-2 imagery. *Remote Sens. Environ.* 102, 390–401. <https://doi.org/10.1016/j.rse.2006.02.022>
- Kelly, R.D., 1982. A single Doppler radar study of horizontal-roll convection in a lake-effect snow storm (Lake-Michigan). *J. Atmos. Sci.* 39, 1521–1531. [https://doi.org/10.1175/1520-0469\(1982\)039<1521:ASDRSO>2.0.CO;2](https://doi.org/10.1175/1520-0469(1982)039<1521:ASDRSO>2.0.CO;2)
- Khanna, S., Brasseur, J.G., 1998. Three-dimensional buoyancy and shear-induced local structure of the atmospheric boundary layer. *J. Atmos. Sci.* 55, 710–743. [https://doi.org/10.1175/1520-0469\(1998\)055<0710:TDBASI>2.0.CO;2](https://doi.org/10.1175/1520-0469(1998)055<0710:TDBASI>2.0.CO;2)
- 595 Klein, A., Ravetta, F., Thomas, J.L., Ancellet, G., Augustin, P., Wilson, R., Dieudonné, E., Fourmentin, M., Delbarre, H., Pelon, J., 2019. Influence of vertical mixing and nighttime transport on surface ozone variability in the morning in Paris and the surrounding region. *Atmos. Environ.* 197, 92–102. <https://doi.org/10.1016/j.atmosenv.2018.10.009>
- Kropfli, R.A., Kohn, N.M., 1978. Persistent horizontal rolls in the urban mixed layer as revealed by dual-Doppler radar. *J. Appl. Meteorol.* 17, 669–676. [https://doi.org/10.1175/1520-0450\(1978\)017<0669:phritu>2.0.co;2](https://doi.org/10.1175/1520-0450(1978)017<0669:phritu>2.0.co;2)
- 600 Kubat, M., 2017. An Introduction to Machine Learning, An Introduction to Machine Learning. Springer International Publishing. <https://doi.org/10.1007/978-3-319-63913-0>
- Kunkel, K.E., Eloranta, E.W., Weinman, J.A., 1980. Remote determination of winds, turbulence spectra and energy dissipation rates in the boundary layer from lidar measurements. *J. Atmos. Sci.* 37, 978–985. [https://doi.org/10.1175/1520-0469\(1980\)037<0978:rdowts>2.0.co;2](https://doi.org/10.1175/1520-0469(1980)037<0978:rdowts>2.0.co;2)
- 605 LeMone, M., 1972. The structure and dynamics of the horizontal roll vortices in the planetary boundary layer. *J. Atmos. Sci.* 30, 1077–1091. [https://doi.org/10.1175/1520-0469\(1973\)030<1077:tsadoh>2.0.co;2](https://doi.org/10.1175/1520-0469(1973)030<1077:tsadoh>2.0.co;2)
- Lemonsu, A., Masson, V., 2002. Simulation of a summer urban breeze over Paris. *Boundary-Layer Meteorol.* 104, 463–490. <https://doi.org/10.1023/A:1016509614936>
- Lhermitte, R.M., 1962. Note on wind variability with Doppler radar. *J. Atmos. Sci.* 19, 343–346.
- 610 Lohou, F., Druilhet, A., Campistron, B., 1998. Spatial and temporal characteristics of horizontal rolls and cells in the atmospheric boundary layer based on radar and in situ observations. *Boundary-Layer Meteorol.* 89, 407–444. <https://doi.org/10.1023/A:1001791408470>
- Newsom, R., Calhoun, R., Ligon, D., Allwine, J., 2008. Linearly organized turbulence structures observed over a suburban area by Dual-Doppler lidar. *Boundary-Layer Meteorol.* 127, 111–130. <https://doi.org/10.1007/s10546-007-9243-0>
- 615 Reinking, R.F., Doviak, R.J., Gilmer, R.O., 1981. Clear-air roll vortices and turbulent motions as detected with an airborne gust probe and dual-Doppler radar. *J. Appl. Meteorol.* 20, 678–685. [https://doi.org/10.1175/1520-0450\(1981\)020<0678:CARVAT>2.0.CO;2](https://doi.org/10.1175/1520-0450(1981)020<0678:CARVAT>2.0.CO;2)
- Saint-Pierre, C., Becue, V., Diab, Y., Teller, J., 2010. Case study of mixed-use high-rise location at the Greater Paris scale. *WIT Trans. Ecol. Environ.* 129, 251–262. <https://doi.org/10.2495/SC100221>
- 620 Sandeepan, B.S., Rakesh, P.T., Venkatesan, R., 2013. Observation and simulation of boundary layer coherent roll structures

- and their effect on pollution dispersion. *Atmos. Res.* 120–121, 181–191. <https://doi.org/10.1016/j.atmosres.2012.08.016>
- Sokolov, A., Dmitriev, E., Gengembre, C., Delbarre, H., 2020. Automated classification of regional meteorological events in a coastal area using in-situ measurements. *J. Atmos. Ocean. Technol.* JTECH-D-19-0120.1. <https://doi.org/10.1175/JTECH-D-19-0120.1>
- 625 Soldati, A., 2005. Particles turbulence interactions in boundary layers. *ZAMM* 85, 683–699. <https://doi.org/10.1002/zamm.200410213>
- Srivastava, D., Rajitha, B., Agarwal, S., Singh, S., 2018. Pattern-based image retrieval using GLCM. *Neural Comput. Appl.* 1–14. <https://doi.org/10.1007/s00521-018-3611-1>
- Stull, R.B., 1988. *An introduction to boundary layer meteorology*. Kluwer Academic Publishers.
- 630 Träumner, K., Damian, T., Stawiarski, C., Wieser, A., 2015. Turbulent structures and coherence in the atmospheric surface layer. *Boundary-Layer Meteorol.* 154. <https://doi.org/10.1007/s10546-014-9967-6>
- Troude, F., Dupont, E., Carissimo, B., Flossmann, A.I., 2002. Relative influence of urban and orographic effects for low wind conditions in the Paris area. *Boundary-Layer Meteorol.* 103, 493–505. <https://doi.org/10.1023/A:1014903627803>
- Tur, A. V., Levich, E., 1992. The origin of organized motion in turbulence. *Fluid Dyn. Res.* 10, 75–90.
- 635 [https://doi.org/10.1016/0169-5983\(92\)90009-L](https://doi.org/10.1016/0169-5983(92)90009-L)
- Vasiljević, N., Lea, G., Courtney, M., Cariou, J.-P., Mann, J., Mikkelsen, T., 2016. Long-Range WindScanner System. *Remote Sens.* 8, 896. <https://doi.org/10.3390/rs8110896>
- Weckwerth, T.M., Horst, T.W., Wilson, J.W., 1999. An observational study of the evolution of horizontal convective rolls. *Mon. Weather Rev.* 127, 2160–2179. [https://doi.org/10.1175/1520-0493\(1999\)127<2160:AOSOTE>2.0.CO;2](https://doi.org/10.1175/1520-0493(1999)127<2160:AOSOTE>2.0.CO;2)
- 640 Weckwerth, T.M., Parsons, D.B., 2006. A review of convection initiation and motivation for IHOP_2002. *Mon. Weather Rev.* <https://doi.org/10.1175/MWR3067.1>
- Wilson, R.B., Start, G.E., Dickson, C.R., Ricks, N.R., 1976. Diffusion under low windspeed conditions near Oak Ridge, Tennessee.
- Yang, X., Tridandapani, S., Beitler, J.J., Yu, D.S., Yoshida, E.J., Curran, W.J., Liu, T., 2012. Ultrasound GLCM texture analysis of radiation-induced parotid-gland injury in head-and-neck cancer radiotherapy: An *in vivo* study of late toxicity. *Med. Phys.* 39, 5732–5739. <https://doi.org/10.1118/1.4747526>
- 645 Young, G.S., Kristovich, D.A.R., Hjelmfelt, M.R., Foster, R.C., 2002. Rolls, streets, waves, and more: A review of quasi-two-dimensional structures in the atmospheric boundary layer. *Bull. Am. Meteorol. Soc.* [https://doi.org/10.1175/1520-0477\(2002\)083<0997:RSWAMA>2.3.CO;2](https://doi.org/10.1175/1520-0477(2002)083<0997:RSWAMA>2.3.CO;2)
- 650